Palaeogeography, Palaeoclimatology, Palaeoecology 560 (2020) 110032

Contents lists available at ScienceDirect

Palaeogeography, Palaeoclimatology, Palaeoecology

journal homepage: www.elsevier.com/locate/palaeo

Changing depocentre environments of Palaeolake Olduvai and carbonates as marker horizons for hiatuses and lake-level extremes

Ian G. Stanistreet[a,b,*], Connor Doyle[a,c], Tom Hughes[a], Elisabeth D. Rushworth[a], Harald Stollhofen[d], Nicholas Toth[b], Kathy Schick[b], Jackson K. Njau[b,e]

[a] Dept. Earth, Ocean and Ecological Sciences, University of Liverpool, Brownlow Street, Liverpool L69 3GP, UK
[b] The Stone Age Institute, Bloomington, IN 47407-5097, USA
[c] School of Earth and Environmental Sciences, University of Manchester, UK
[d] GeoZentrum Nordbayern, Friedrich-Alexander-University (FAU) Erlangen-Nürnberg, Schloßgarten 5, 91054 Erlangen, Germany
[e] Department of Earth and Atmospheric Sciences, Indiana University, 1001 East 10th Street, Bloomington, IN 47405-1405, USA

ARTICLE INFO

Keywords:
Micrite limestone
Dolmicrite layer
$\delta^{13}C$ and $\delta^{18}O$ graph
Magnesium anomaly
Soil profile
Enterolithic nodule

ABSTRACT

Primary carbonate and marl layers and limestone nodular horizons were intersected in OGCP Boreholes 1A, 2A, 3A, 3B, drilled into the depocentre of Palaeolake Olduvai. The various carbonate types were analysed, employing petrographic (including cathodo-luminescence), stable isotope, and sequence stratigraphic techniques, and recorded important information concerning lake evolution.

Primary carbonate and marl layers are preserved at the top of lake deepening cycles (lake-parasequences), marking maximum flooding, followed by lake withdrawal, and then fluvial erosion, leading to the next depositional cycle. Presence of pelagites and a meromict lake favouring anoxic conditions, show it to be not a playa lake, but a deeper fault-bound lake, akin to present day Lake Eyasi. Carbonate and marl layers were exclusively deposited when claystone facies show a geochemical magnesium anomaly associated with a phase of basaltic volcanism affecting the basin, marked by mafic tuffs and basaltic lava flows. Calcium was partitioned into evaporites, such as gypsum/anhydrite, together with the nodular horizons and carbonate soil profiles in the sequence. The resulting high Mg^{2+}/Ca^{2+} ratio in the lake waters promoted dolomite deposition and replacement, and the formation of aragonite.

The nodular horizons yield rainfall isotope values and mark times when the lake was empty and the lake-bed fell under meteoric conditions, precipitating limestone nodules just below the sediment surface under pedogenic vadose, groundwater interface, and groundwater phreatic conditions. The nodular limestone horizons sit below erosional/hiatal surfaces and show vadose micritic and fibrous types to phreatic sparry and other accretionary type textures. Enterolithic to chickenwire textured nodules indicate the pseudomorphing of anhydrite nodules that form beneath salt marshes.

Thus, the two carbonate types, primary layers and nodular horizons, provided depth gauges, respectively for the extremes of lake expansion and emptying/drying out. In the case of nodular horizons, the maturity of the carbonate profile gives an indication of the magnitude of the hiatal time gap represented, ~ 1 kyr to 2 kyr for a single horizon to ~ 3 kyr to 9 kyr for more mature soil profiles. Emptying/drying out episodes of Palaeolake Olduvai were not uncommon, and often short-lived. A spectrum of hiatal disconformities in the Olduvai Basin vary from multimillennial hiatuses to mega-disconformities of ~ 40 kyr and ~ 75 kyr.

1. Introduction

In August 2014, the Olduvai Gorge Coring Project (OGCP), under the auspices of the Stone Age Institute, drilled four boreholes at three sites (Fig. 1) into the depocentre of the Olduvai Basin, through the deepest tracts of Palaeolake Olduvai. The aim was to extract as continuous and extended a core as possible through fine grained lacustrine sediments, recording various facies sequences containing microfossil, biomarker and geochemical proxies (Stanistreet et al., 2020b), to determine palaeoclimatic variation at a time of significant changes in hominin evolution. Detection of palaeoclimate variation is particularly important in a basin where multiple hominin species have been

* Corresponding author at: Dept. Earth, Ocean and Ecological Sciences, University of Liverpool, Brownlow Street, Liverpool L69 3GP, UK.
E-mail address: istanistreet@btconnect.com (I.G. Stanistreet).

https://doi.org/10.1016/j.palaeo.2020.110032
Received 1 June 2019; Received in revised form 16 September 2020; Accepted 16 September 2020
Available online 22 September 2020
0031-0182/

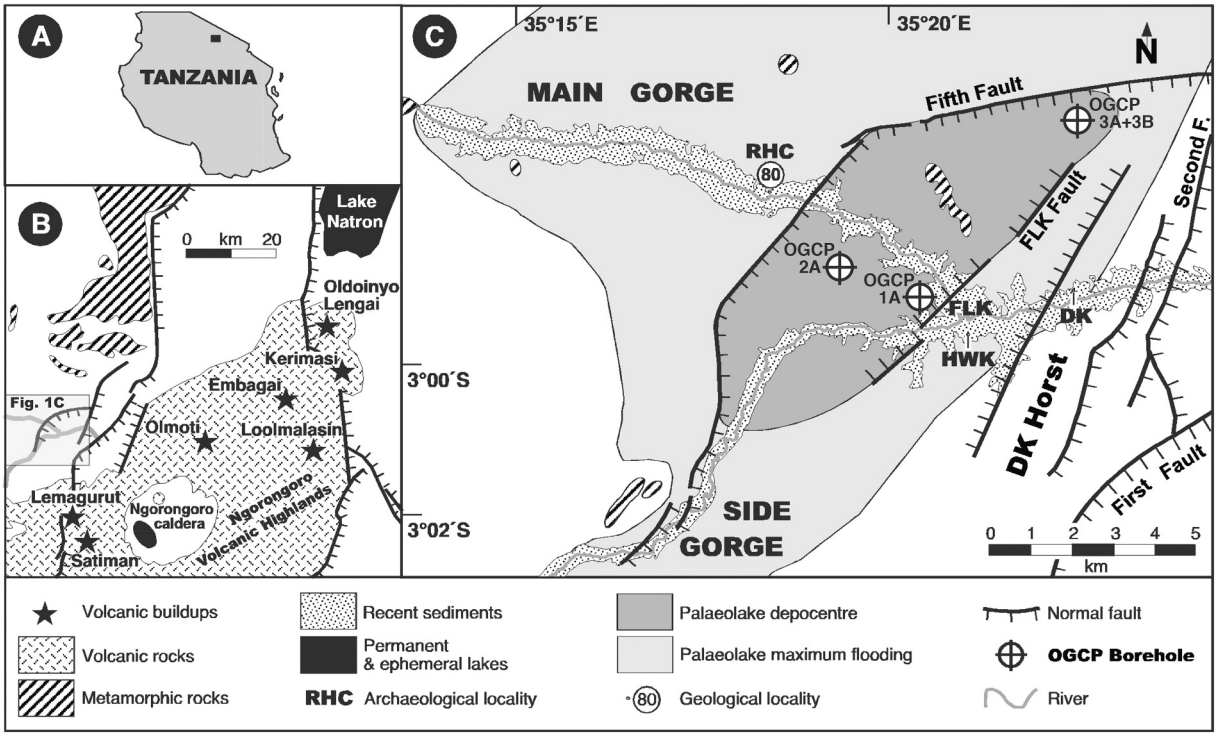

Fig. 1. A. Position of the Olduvai area in northern Tanzania (black rectangle). B. Regional setting of Olduvai Gorge with respect to the Ngorongoro Volcanic Highlands (dashed grey shaded area) and volcanoes mentioned in the text. C. New reconstruction of the position of Palaeolake Olduvai depocentre and area of maximum flooding during deposition of Upper Bed I (Stanistreet et al., 2020a, this volume), with locations of OGCP Boreholes 1A, 2A, 3A & 3B indicated. The depocentre of Palaeolake Olduvai is constrained between Fifth and FLK Faults. Highlighted by capital letters are archaeological sites of Leakey (1971) mentioned in the text. (RHC = Richard Hay Cliff; FLK = Frida Leakey Korongo; HWK = Henrietta Wilfrida Korongo; DK = Douglas Korongo).

excavated in single successions and therefore co-existed prior to extinctions of some species (Leakey, 1971; Leakey and Roe, 1994). The boreholes were necessary because the depocentre of Palaeolake Olduvai between the FLK and Fifth Faults is either not well exposed (Beds II, III, IV), or in the case of older stratigraphy, below Bed II, not exposed at all. To date it has been portrayed (e.g. Maslin et al., 2014) that Palaeolake Olduvai only extended from 1.75 Ma to 1.97 Ma ago, and to test this, the borehole cores were set to penetrate exclusively the lake depocentre to access the entire lake record, and to explore whether there was lake stratigraphy prior to the oldest then known stratigraphy at 2.0 Ma. The resulting core record showed the lake extending from ~2.4 Ma to ~0.4 Ma (Stanistreet et al., 2020a, this volume), with lake sediments absent only for the ~ 100 kyr, during which the Ngorongoro Volcanic fan-delta prograded across the depocentre. Previous attempts at measuring proxies from the palaeolake were undertaken with outcrop samples outside the depocentre that had experienced weathering, which was not a problem with borehole core.

The borehole cores intersected at depth large thicknesses (~135 m) of yet unknown stratigraphy not exposed at surface (Fig. 2). The known and newly discovered stratigraphic levels of the Olduvai Basin are described in Stanistreet et al., 2020a, this volume), and new units, the Ngorongoro Formation (volcano-sedimentary fan-delta deposits sourced from Ngorongoro Volcano) and Naibor Soit Formation (lake and fluvio-deltaic deposits) were introduced, designating the boreholes as type sections. Estimated age of the oldest sediments intersected (Naibor Soit Formation) are ~ 2.25 or ~ 2.45 Ma (Age models C or D of Deino et al., 2020: Fig. 6).

During logging of Cores 1A, 2A, 3A and 3B, it was realised that the positions and types of carbonates within the sequence offered an insight, not only into hiatal breaks, but also times of maximum lake flooding (Stanistreet, 2012). Therefore, we hypothesised that the carbonates are natural markers for lake depth changes and extent. This paper tests that hypothesis in the depocentre of Palaeolake Olduvai. A misconception at times is that central lake sequences tend to be largely continuous if composed of fine grained sedimentary facies. Age-depth models have been constructed and palaeoclimatic records erected that show little or no break in lake sedimentation, particularly in Pleistocene basins. Notable exceptions are Trauth (2014) and Trauth et al. (2015), who identified hiatuses of 3.8 kyr, 9.18 kyr, 20 kyr and 80 kyr duration in the Ol Njorowa (Naivasha Basin) and Olorgesalie sequences. Assumption of a lack of hiatal or unconformable breaks in lake sequences goes against all the previous experience of lake basin successions in older stratigraphies. Also, in other Pleistocene basins, lake sediments can be shown to have undergone pronounced desiccation, erosion and soil formation (e.g. Lake Malawi, Cohen et al., 2007; Scholz et al., 2007). Clearly techniques are required in Pleistocene basins to identify the timing and extent of sedimentary hiatuses on all scales, in order that accurate age-depth models might be constructed and the true nature of the proxy palaeoclimatic records discerned.

2. Geological setting

The Olduvai Basin was a closed basin throughout almost its entire history, only occasionally was there a possible connection with the neighbouring Lake Natron Basin (Fig. 1B, C), due to tectonism (Hay, 1976). The basinal depocentre developed between the master detachment Fifth Fault, an extensional displacement along which the entire basin subsided (Stollhofen and Stanistreet, 2012), and the FLK Fault, representing the northwestern edge of the DK Horst (Fig. 1C) (Stollhofen and Stanistreet, 2012), which also rode on the Fifth Fault detachment surface and bounded the southeastern margin of the lake for long periods. Lake facies are characterised by olive “waxy” (smectitic) claystones (Hay, 1976; Stanistreet et al., 2018a) and sandy “waxy” (smectitic) claystones (Stanistreet et al., 2018a), and also comprise primary carbonate layers that are one subject of this paper.

Throughout its history major providers of coarse siliciclastics

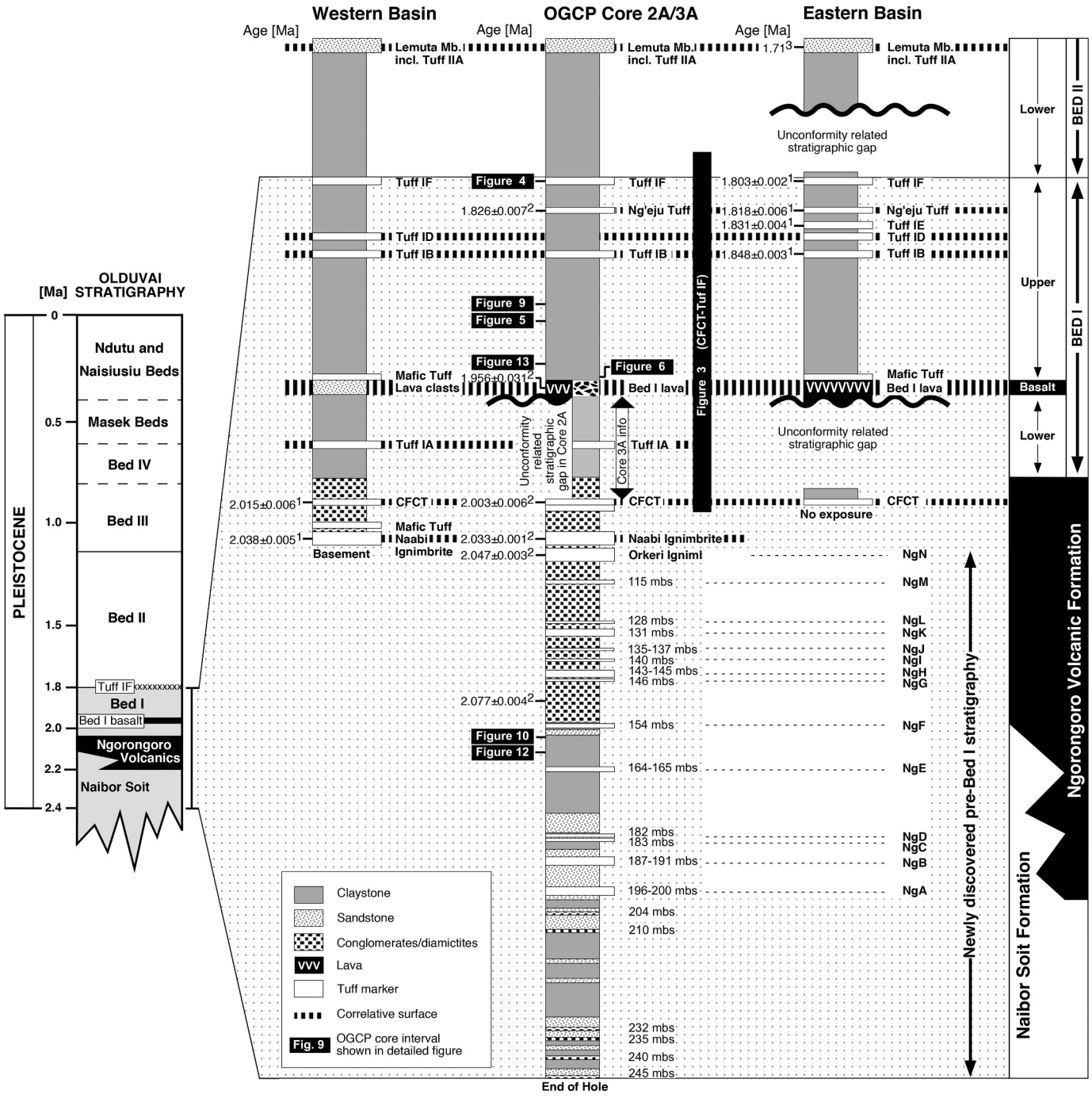

Fig. 2. Generalized Olduvai Basin stratigraphy (left column), based on Hay (1976) with newly discovered pre-Bed I strata (Naibor Soit and Ngorongoro Volcanic Formations) of OGCP Cores 2A/3A (Stanistreet et al., 2020a, this volume). The latter is compared to western and eastern Olduvai Basin stratigraphies, compiled from outcrop measurements. Both sections are representative for areas ~4 km distant from the OGCP 2A borehole location towards WNW and ESE. Dashed lines indicate proposed correlative surfaces between tephrostratigraphic markers (McHenry et al., 2020a, this volume). NgA to NgQ labels indicate positions of marker tuffs (Tuff NgO = Naabi Ignimbrite. NgQ = CFCT ignimbrite) in the Ngorongoro Formation (middle and right column). Stratigraphic positions of detailed figures are indicated and highlighted by black boxes. Dates are from [1]Deino (2012: $^{40}Ar/^{39}Ar$ dating), [2]Deino et al., 2020. (this volume). and [3]Curtis and Hay (1972).

(conglomerates, sandstones, volcaniclastic sandstones, diamictites) into the basin were the developing Ngorongoro Volcanic Highlands, a complex of volcanoes that has proceeded to develop from the Pliocene to the present day, largely extending towards the northeast as the Olduvai Basin subsided and evolved. From ~2.2 Ma to 2.0 Ma, Ngorongoro Volcano itself (Fig. 1) developed to the southeast of the basin (Mollel and Swisher III, 2012) and sourced a fan-delta that prograded across the lake depocentre (Stanistreet et al., 2020a, this volume). Then Olmoti Volcano (Fig. 1) developed to the east of the lake, between ~1.85 Ma and 1.80 Ma during the deposition of Bed I, but the Olmoti Fan prograded only to the west of the DK Horst as far as Borehole 1A (Stanistreet et al., 2020a, this volume). Volcanoes Loolmalasin, Embagai and Kerimasi then evolved successively further towards the northeast, supplying coarse sediments variously to Beds II, III, IV and Masek Beds (Hay, 1976; Stanistreet et al., 2020a, Stanistreet et al., 2020b this volume). Primary volcanic products were also commonly deposited at various times within the basin, including basaltic lava flows and pyroclastic flow, surge and airfall tuffs (Stollhofen et al.,

2008; Blumenschine et al., 2012b, 2012a). Particular Tuff Markers have been distinguished (Fig. 2), including the Naabi Ignimbrite, Coarse Feldspar Crystal Tuff (CFCT), Tuff IA, all derived from Ngorongoro Volcano, and Tuffs IB, IC, ID, IE, Nge'ju and IF, derived from Olmoti Volcano (McHenry, 2012; McHenry et al., 2020a). Tephrostratigraphic markers and unconformity surfaces were preferentially used by Hay (1976) to subdivide the Plio-Pleistocene succession of Olduvai Gorge into seven Formations (Beds I–IV, Masek Beds, Ndutu Beds, and Naisiusiu Beds), overlying a crystal-rich tuff termed the Naabi Ignimbrite (Fig. 2). Only during the course of the Olduvai Gorge Coring Project (OGCP) was an extra 135 m of new stratigraphy discovered beneath the Naabi Ignimbrite (Stanistreet et al., 2020a, this volume), labelled as "pre-Bed I stratigraphy", involving the lacustrine dominated Naibor Soit Formation and the fan-delta dominated Ngoronogoro Volcanic Formation (Fig. 2).

3. Previous reports and analyses of carbonates from the Olduvai Beds

Carbonates were originally recorded in the Olduvai Beds by Hay (1976). He distinguished the following types: limestone nodules, limestone layers (some ooidal), dolomite layers, algal limestones, calcite crystals and calcrete layers. Cerling and Hay (1986) undertook pioneering $\delta^{13}C$ and $\delta^{18}O$ isotope analyses of Olduvai carbonates, distinguishing covariant isotope trends in what were differentiated as pedogenic/calcrete-forming, fluvially related pedogenic, non-pedogenic, and, separately, authigenic lake calcite crystals. In their investigation of the chemical sedimentology of Palaeolake Olduvai, Hay and Kyser (2001) identified four dolostone layers from Bed I and Lower Bed II at RHC (Richard Hay Cliff, Loc. 80) in the western Olduvai Gorge (Fig. 1), on the upthrown side (footwall block) of Fifth Fault, outside the depocentre.

Bennett et al. (2012) undertook further $\delta^{13}C$ and $\delta^{18}O$ isotope analyses on the nodular types of carbonate, which vary from individual to amalgamated nodules that continue laterally to approximate an irregularly shaped layer. They found that covariant trends were not only present from samples throughout the sequence, but also within an individual nodule. These they interpreted as mixing trends during the formation of a nodule relating to the admixture of freshwater groundwaters with underlying denser saline-alkaline lake waters. A similar process had been proposed by Liutkus et al. (2005) to explain isotope analyses of calcareous rhizoliths, but this required the lighter freshwater groundwaters to penetrate below the denser saline groundwater.The OGCP drilling intersected many types of carbonates, both primary sedimentary layers and nodular bodies. Features recognised could be used to test previous hypotheses.

Ashley et al. (2014b) identified four carbonate layers, including both nodular and primary depositional layers: below Tuff IB, Tuff IC, and Tuff IF (see Stanistreet et al., 2020b, their Fig. 7) and another above Tuff IID. They interpreted these as marking drier phases during Milankovitch cyclicity, although the carbonates formed according to rather differing processes.

4. Methods

Boreholes were drilled using an Atlas Copco CS 14 Diamond Core Drill Rig with HQ3 surface set core bits (3.872″ x 2.400″). Borehole 1A (S 02° 59′ 08.2″ E 035° 20′ 34.1″) extends 85 m, just through the Bed I Basalt; Borehole 2A (S 02° 57′ 13.9″ E 035° 15′ 33.2″) extends 245 m, intersecting 135 m of previously unknown strata beneath Bed I; Boreholes 3A & 3B (S 02° 56′ 41.6″ E 035° 22′ 51.5″) extend 135 m and 147 m respectively, also into newly discovered strata. Core intervals were airfreighted to the LacCore facility in Minneapolis. There the cores were split into two halves, designating: an Archive, A, half, for imaging, logging and conserving; and a Working, W, half for sampling. Samples were given the LacCore code, e.g. OGDP-OLD14-2A-36Y-2-A (=PROJECT-LOCATION/DATE-BOREHOLE NO.-CORE RUN-CORE INTERVAL-ARCHIVE/WORKING). For brevity the sample numbers referred to in this paper will be recorded by the shortened form, such as 2A-36Y-2, followed, if necessary, by the centimetre position within that core interval. Logging was undertaken using Corelyzer and Psicat software, developed for LacCore. Results were presented as pdf books of the actual logging and a computer-generated stratigraphy for the entire core. During logging, lithofacies were identified according to a pro forma scheme available in Psicat. The lithofacies were sampled for thin section, cathodo-luminescence and isotope analyses. Oxygen and carbon stable isotope analyses of carbonate lithotypes were carried out using 5 mg samples for bulk analyses and 10 μg samples for precision analyses. Isotopic analysis was undertaken using a modified VG Sira mass spectrometer at the University of Liverpool Stable Isotope Laboratory to produce values of $\delta^{13}C$ and $\delta^{18}O$. Data were corrected using standard procedures and isotopic values are shown relative to the Vienna Pee Dee Belemnite (VPDB) international scale, with an analytical uncertainty of < 0.1‰ for both carbon and oxygen isotopes.

5. Results

Sedimentary facies logged in the OGCP boreholes varied from conglomerates, through sandstones and volcaniclastic sandstones, to sandy claystones and claystones. Associated with the latter two facies were the micrite or dolmicrite layers which are one of the major themes of this paper. Primary volcanic facies units within the sequence were assigned to devitirified, vitric or crystal and vitric tuffs according to the Psicat scheme, but whether the tuffs were lapilli, coarse/fine ash, ash lapilli or lapilli ash tuffs was recorded in the descriptive notes, together with maximum grain size and unit thickness. Diamictites and sandy diamictites were other, but reworked volcanic facies encountered in the core, lahar or volcanic mudflow deposits, as described from outcrops by Stanistreet (2012), Stanistreet et al., 2018b, 2018a and de la Torre et al. (2018).

5.1. Principal types of Palaeolake Olduvai carbonates

Various carbonate bodies were intersected in the borehole cores and two basic geometric forms were sampled: layers of primary carbonate composed of micritic dolomite (dolostone) or limestone; and nodular to more continuous nodular carbonates that comprise only limestone.

Primary carbonate or marl layers are usually interbedded with claystone or sandy claystone facies within Bed I of the Olduvai Beds. These carbonate and marl layers comprise either dolomite or limestone components, with micritic textures dominating. Dolomite layers have also commonly been detected and measured (see Stanistreet et al., 2020b, their Fig. 7) in the lake marginal areas of Palaeolake Olduvai (see particularly Hay, 1976; Hay and Kyser, 2001; Stanistreet, 2012; Bennett et al., 2012; Rushworth, 2012).

Nodular carbonate horizons were developed quite commonly within the Olduvai Basin cores' sequences. It was decided that nodule styles and isotopic signatures should be studied more systematically and compared to the record of nodules established previously from the lake marginal areas (Bennett et al., 2012; Rushworth, 2012; Ashley et al., 2014a).

A third type of primary carbonate depositional layer was frequently logged in the three cores. Generally thin (< 5 cm) and usually sand and silt grade, such calcarenites comprise mostly accumulations of authigenic calcite crystals, and rarely ooids, reworked from those precipitated within the shallows and shallow subsurface of the lake (reported by Hay, 1976; Cerling and Hay, 1986; Hay and Kyser, 2001; Rushworth, 2012). Such layers often show grading and usually represent turbidity current deposits, formed when density currents transported the coarser material from the shallow lake into the lake depths. Alternatively, accumulations of calcite crystals can develop as erosive lags. They are not useful to gauge depth of deposition and will not be dealt with further in this paper.

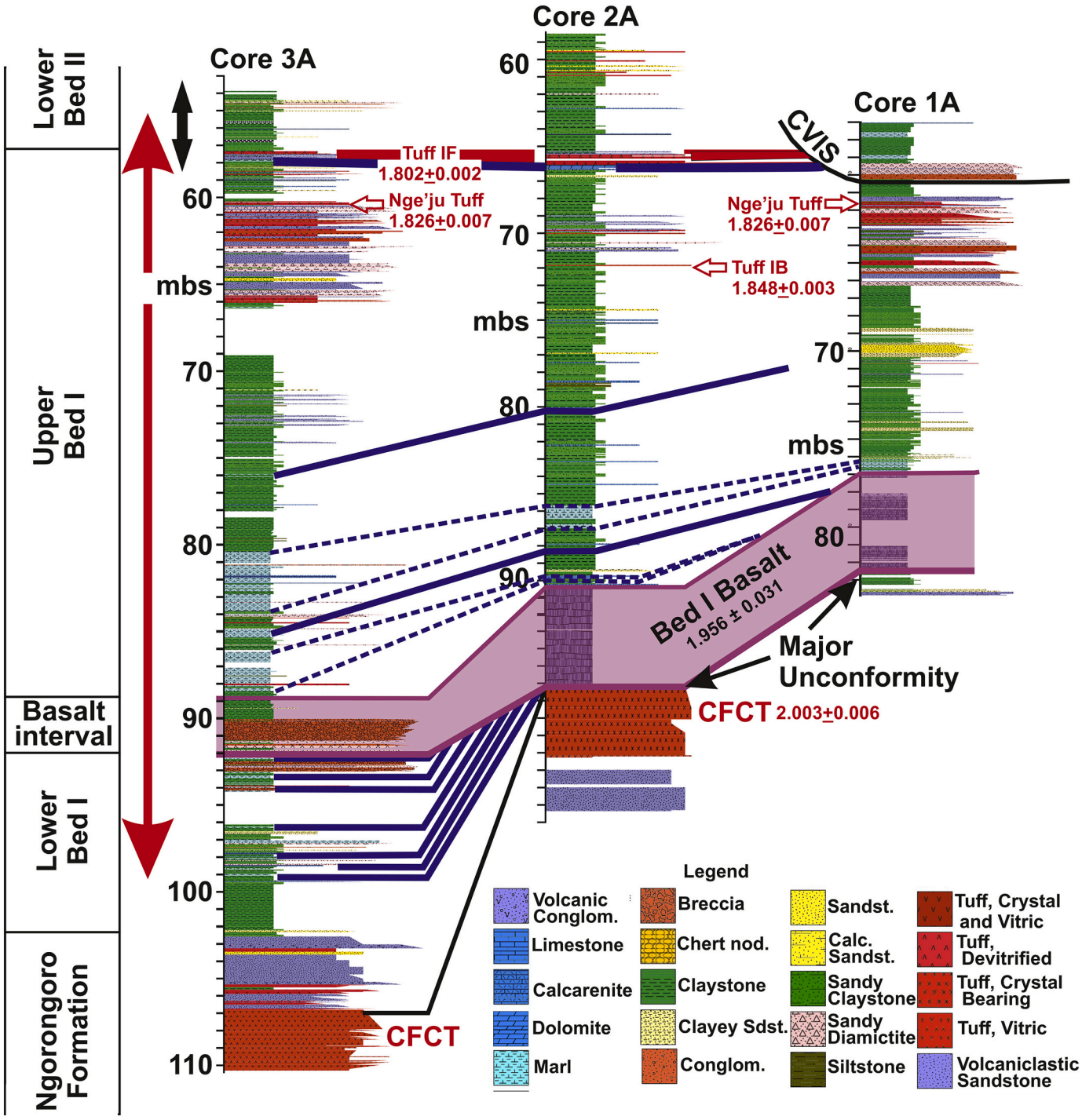

Fig. 3. Dolostone and limestone layers deposited during the claystone Mg-anomaly of Bed I (stratigraphic range of anomaly in Core 3A indicated by the double ended vertical red arrow (see Stanistreet et al., 2020b, this volume). Dashed blue lines = top and bottom of major carbonate units; solid blue lines = correlation of thinner carbonate units. The carbonate immediately below Tuff IF can be seen in outcrop at RHC (Loc. 80) (see Stanistreet et al., 2020b their Fig. 7; stratigraphic extent indicated here by vertical double ended black arrow). Note that Lower Bed I is missing in Cores 1A and 2A, due to a major disconformable hiatus, and Tuff IF is removed in Core 1A by the Crocodile Valley Incision Surface (CVIS) (Stanistreet, 2012; Stanistreet et al., 2018b, Stanistreet et al., 2020a this vol) (mbs = metres below surface). Dates from Deino (2012) and Deino et al., 2020 (For interpretation of the references to colour in this figure legend, the reader is referred to the web version of this article.)

5.2. Carbonate layers in OGCP Cores 1A, 2A, 3A

Fig. 3 shows the position of primary micritic carbonate and marl layers within the borehole stratigraphic profile (light blue = marl layer; dark blue = limestone or dolostone (dolomite) layer, depending upon standard ornamentation). It should be noted that the layers are restricted to Bed I (revised stratigraphy of Stanistreet et al., 2020a, this volume), and do not appear in lacustrine facies of any of the other Beds. This has been explained from the geochemical perspective because the primary carbonates are only laid down during a period when claystone geochemistries display anomalously high magnesium concentrations (range indicated by vertical double ended red arrow in Fig. 3)

(Stanistreet et al., 2020b, this vol). Magnesian flushing of Palaeolake Olduvai can be related (Stanistreet et al., 2020b, this volume) to the basaltic magmatism associated with the terminal phase of bimodal Ngorongoro volcanism, when basaltic magmas were accessed for extrusion at surface by enhanced extensional tectonics, causing enhanced basin subsidence. Mafic Tuffs, the Bed I Basalt lavas and basaltic scoria-bearing layers all witness this stage in basinal evolution. Fig. 3 illustrates the details of Bed I stratigraphy in all three boreholes, with major carbonate units outlined by dashed blue lines and correlation of thinner carbonate units indicated by solid blue lines.

Fig. 3 further shows why Lower Bed I and its contained carbonate layers are only preserved in Cores 3A and 3B, whereas they are cut out by a disconformity in Cores 1A and 2A. Age determinations (Deino, 2012; Deino et al., 2020; Stanistreet et al., 2020b, this vol) show that the time missing on this surface in Core 2A amounts to ~ 75 kyr. Also, Tuff IF and underlying dolmicrite layer are missing in Core 1A, removed by the Crocodile Valley Incision Surface (CVIS) (Stanistreet, 2012; Stanistreet et al., 2018b, Stanistreet et al., 2020a, this vol). Lake-parasequence analysis (Stanistreet, 2012) suggests that ~ 40 kyr of stratigraphy are cut out by the CVIS disconformity at the Borehole 1A location.

The uppermost of the carbonate units logged is a dolmicrite to dolomitic marl immediately below Tuff IF (Figs. 2 and 4) just referred to, which is the ultimate primary micritic carbonate in the basin history. An outcrop correlative of the unit from Geological Locality 80 (Fig. 1) is pictured in Stanistreet et al., 2020b, their Fig. 7), within a sequence whose stratigraphic position is located on Fig. 3 (double ended black arrows). The same carbonate unit is shown in more detail in the core logs of Fig. 4 (within the sub-Tuff IF maximum flooding zone, highlighted in light blue), varying between dolmicrite in Core 2A to dolomitic marl in Core 3A. The unit records the maximum flooding surface (Stanistreet, 2012) in a deepening trend associated with the lake-parasequence immediately below Tuff IF, documented in outcrop stratigraphic profiles by Bamford et al. (2008), Stanistreet (2012) and Stollhofen and Stanistreet (2012). The lake-parasequence above, which includes Tuff IF, is also shown, including the lowermost part of Lower Bed II, as recorded by Stanistreet (2012), Stollhofen and Stanistreet (2012) and Blumenschine et al., 2012b. The incision surface at the base of this lake-parasequence cuts down into the top of the carbonate unit in Core 2A, but a 1 cm thick unit of “butter” claystone (stevensite-rich claystone described first by Hay and Kyser, 2001) is preserved below the incision surface and above the carbonate unit in Core 3A, which would correlate with the butter claystone recorded at Site HWK (= Henrietta Wilfrida Korongo) (Fig. 1) in Fig. 21 by Stollhofen et al. (2008) and Fig. 2 by Bamford et al. (2008). Thus, that stevensitic clay unit must have been deposited throughout the basin, and so is far more widespread than has been previously realised.

Below Tuff IB, lower down in Upper Bed I (between 75 mbs and 90 mbs in Core 3A; 70 mbs and 90 mbs in Borehole 2A), are a series of carbonate and marl layers, both thickly and thinly developed (Fig. 3). One such unit from core interval 2A-33Y-2 is shown in detail in Fig. 5 at a depth between 80.1 mbs to 80.4 mbs in Borehole 2A. The micritic limestone grades upward from an underlying massive olive waxy claystone and is topped by a sharp erosive surface. In all cases the carbonate layers thicken and become more numerous according to their proximity to Fifth Fault (to the left in Fig. 3), which was the major detachment upon which the Olduvai Basin subsided (Stollhofen and Stanistreet, 2012; Lu et al., 2019, this vol).

Near the bottom of Upper Bed I in Cores 1A and 2A, a limestone unit occurs almost immediately above the Bed I Basalt. No pillow lava features or hyaloclastites are evident at or below the basalt lava contacts with the sedimentary sequence. Stromatolitic lamination was developed in the limestone, exhibiting slight domical geometries (Fig. 6), and the unit was one of the first to be deposited above the basalt, once the basalt had been flooded by Palaeolake Olduvai. Thin sections of the unit reveal bird's-eye structures (Shinn, 1968), voids that have developed between individual stromatolitic laminae.

In Lower Bed I (Fig. 3), seven thin carbonate layers are developed in Core 3A following the onset of the magnesium anomaly (vertical double headed red arrow to the left of and between 55 mbs and 98 mbs in Core 3A in Fig. 3) (Stanistreet et al., 2020b), but prior to the extrusion of the basalt. One of these carbonates, the second upwards, deserves special mention. It is a limestone developed immediately above Tuff IA (Stanistreet et al., 2020b, their Fig. 9) and is figured and described by Hay (1976), who describes ooidal facies from that unit in the western Olduvai Gorge outcrops. The Lower Bed I sequence containing these thin carbonate layers is missing from Boreholes 1A and 2A.

5.3. Carbonates as nodular precipitates in Cores 1A, 2A, 3A, 3B

Arrows in Fig. 7 indicate the positions of nodules studied and analysed within the four cores. As recognised by Bennett et al. (2012) from Palaeolake Olduvai marginal areas, such nodular horizons are frequently associated with overlying erosional or hiatal surfaces. Fig. 7 shows that such nodules occur throughout all the beds intersected in the four boreholes, including the newly discovered pre-Bed I strata. The nodules range between 2 cm and 20 cm in size, are spherical to irregular in shape, and their growth textures are variable. Broadly, they exhibit: either no apparent textures nor any identifiable circumgranular structures; or poor to well-defined layers of calcite radiating conically from a central nucleus, with individual calcite layers < 0.2 mm in thickness. A characteristic feature of many of the nodular carbonates is that they contain inclusions of angular to sub-rounded detrital siliciclastic and detrital carbonate material of various grain sizes, and the intrinsic textures of both structureless and accretionary nodules are often cross-cut by late generations of secondary sparry calcite and dolomite cements, occurring within randomly-oriented fractures. In thin section, these carbonates display much more complex textures, but they can broadly be categorised variously as micritic, spherulitic or sparry (Rushworth, 2012). Nodules were chosen to be described here from four positions within the borehole cores, to encompass the variety that was encountered and to best represent the palaeohydrological environments that were present during the Pleistocene evolution of the deepest portion of Palaeolake Olduvai.

Fig. 8 plots $\delta^{13}C$ against $\delta^{18}O$ values for all nodules studied from the four OGCP cores. They display a degree of deviation, but are arranged in a broadly covariant trend. $\delta^{13}C$ values range between −7.0‰ and 3.0‰ whilst $\delta^{18}O$ values range between −7.5‰ and 0.5‰. There is a linear covariance between $\delta^{13}C$ and $\delta^{18}O$ for the majority of values, particularly in nodules from Core 2A, and a secondary univariant trend of increasing $\delta^{13}C$ in several nodular carbonates from Cores 3A and 3B.

A large (7.5 cm diameter) accretionary nodule is shown in Fig. 9, similar to those described by Bennett et al. (2012) as “cannonball” nodules. The nodule is largely micritic and contains inclusions of siliciclastic and carbonate material up to silt-grade, having developed in a sandy claystone unit that grades upward from the underlying claystone. Detrital material, commonly visible to the naked eye in specimen, can also be seen in abundance in thin section, and comprises a mixture of angular quartz, feldspar and carbonate grains within a clay and fine sand grade matrix. An erosion surface developed in the sequence above the nodule has incised to the degree that the top of the nodule is just truncated by that erosion. The sandy clay that was deposited on top of the erosion surface contains two thin 15 mm and 10 mm calcarenite layers, one of which is normally graded with a load casted base, suggesting rapid fallout.

Another horizon of nodules is shown in Fig. 10, with optical and cathodoluminescence photomicrographs of some of these nodules depicted in Fig. 11A, A1, B and B1. In thin section, the nodules contain an abundance of displacing, euhedral spherulitic and often fibrous calcite grains occurring in situ within a micrite-calcite spar matrix. The distribution of calcite growths, cements and other void-filling carbonate material can be distinguished from detrital, non-calcareous angular to

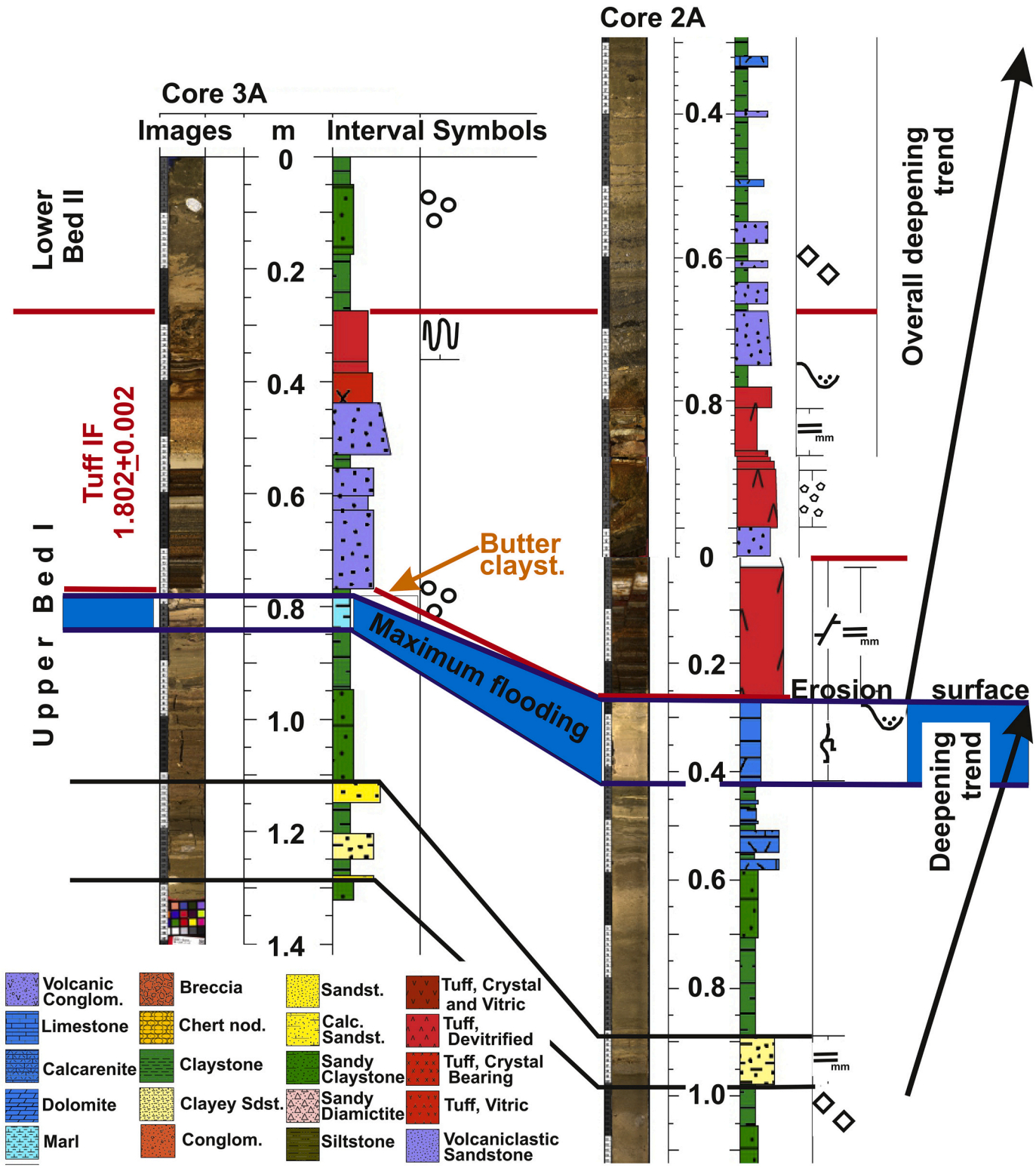

Fig. 4. Correlation of the dolmicrite immediately beneath Tuff IF in Borehole 2A (see Fig. 2 for stratigraphic position) to the calcareous marl in Borehole 3A (Core intervals 2A-28Y-1; 2A-28Y-2; 2A-29Y-1; 3A-24Y-1). The unit also correlates at surface to the dolmicrite exposed at RHC (Loc. 80) (see Stanistreet et al., 2020b their Fig. 7). Like the last, a thin claystone sits above the marl, but the unconformity below Tuff IF cuts down slightly into the dolmicrite of Borehole 2A. The unit marks the top of the deepening trend of a lake-parasequence (Stanistreet, 2012). For meanings of symbols see other figure legends.

sub-rounded clasts when viewed in cathodoluminescence. A pronounced erosion surface is present about 15 cm above the top of the nodular layer, overlain by a volcaniclastic sandstone.

A group of several small (< 3 cm) carbonate nodules is illustrated in Fig. 12, in a horizon intersected in core interval 2A-62Y-2 of Borehole 2A, within the Naibor Soit Formation (Stanistreet et al., 2020a, this volume). These nodules are developed within a greenish-brown, "waxy" claystone. They illustrate mixed micrite-spar fabrics in hand specimen and are commonly irregular to spherical in shape. Fig. 11C, C1, shows photomicrographs of Sample 2A-62Y-2 (20–27 cm), collected from the

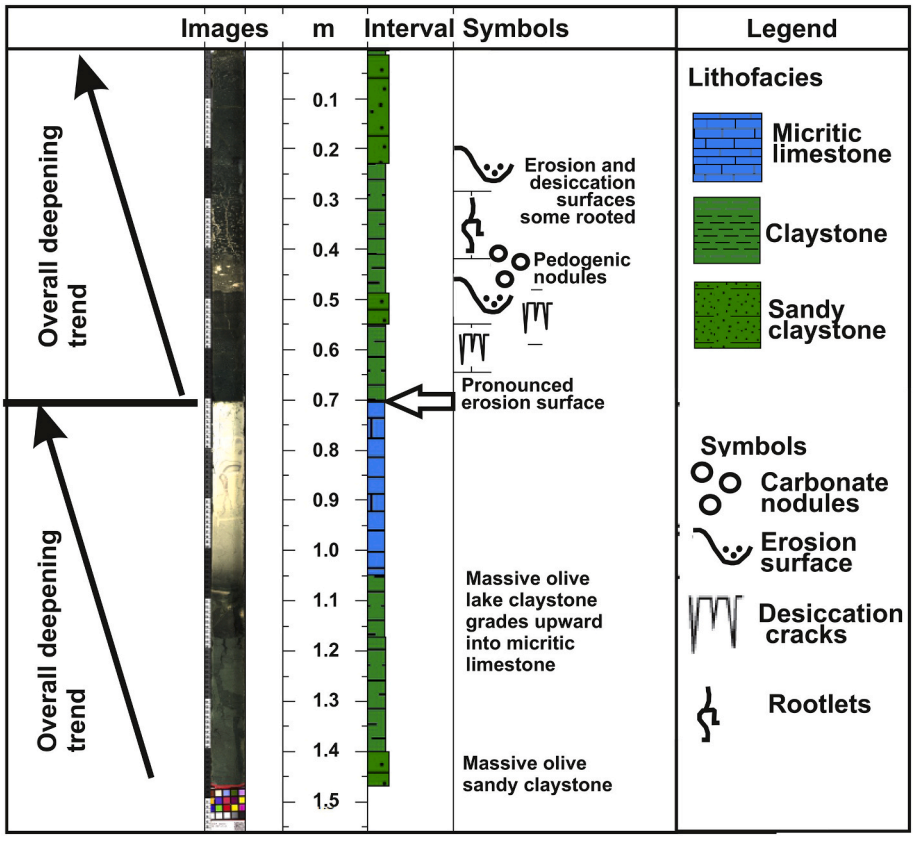

Fig. 5. A good example of a primary carbonate, in this case a micritic limestone, layer in Upper Bed I below Tuff IB (OGDP-OLD-2A-33Y-2-A; see Fig. 2 for stratigraphic position), with bottom gradational with underlying massive claystone and a sharp eroded top. Above the erosion surface are claystones displaying occasional shallow water or emersion structures, including erosion surfaces, desiccation cracks, rootlets and pedogenic carbonate nodules.

horizon, and illustrates textures occurring within the nodules that suggest their development in situ. Poorly to well-formed displacing radial and fibrous calcite grains are abundant when viewed in thin section. Fig. 11D and D1 are photomicrographs from a nodule, Sample 2A-67Y-2 (60 cm–73 cm) at 176 mbs depth in Core 2A, showing strong alveolar textures.

A rather specific type of nodular texture (Fig. 13), with forms not previously encountered in the Olduvai Basin, was intersected in Borehole 2A at a depth of 88.3 mbs. Now comprising micrite, these are irregular nodular intergrowths whose textures are termed by Hussain and Warren (1989) enterolithic and chickenwire types.

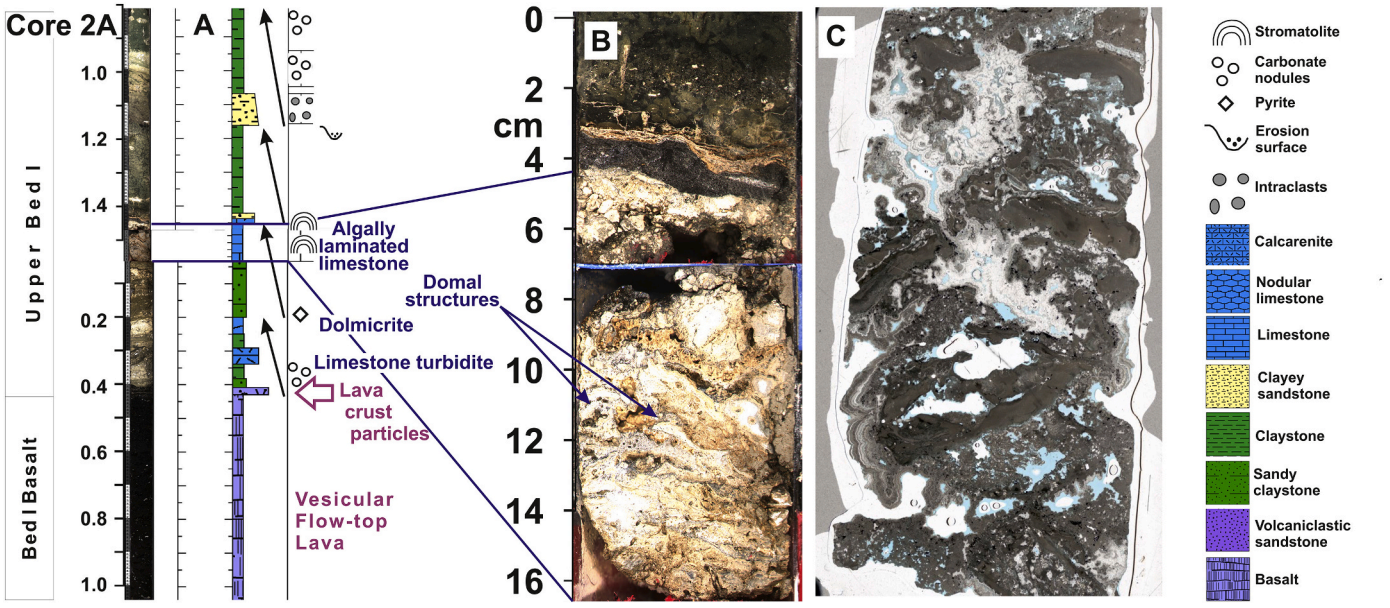

Fig. 6. A. Domal stromatolitic structures in a limestone unit above the Bed I Basalt, intersected in Core 2A (OGDP-OLD-2A-36Y2A to 2A-37Y-1A; see Fig. 2 for stratigraphic position). B. Detailed image showing domal structures. C. Thin section in plane-polarised light, scale bar = 10 mm (blue colour = impregnation of pore space with coloured resin adhesive, to stabilise the rock during thin section preparation). Note the bird's-eye structures. Laminae produced by cyanobacterial mats in a lake shoreline setting. The basalt top shows no evidence of lava interaction with water, so the sedimentary sequence onlapped onto the basalt unit after a hiatus. (For interpretation of the references to colour in this figure legend, the reader is referred to the web version of this article.)

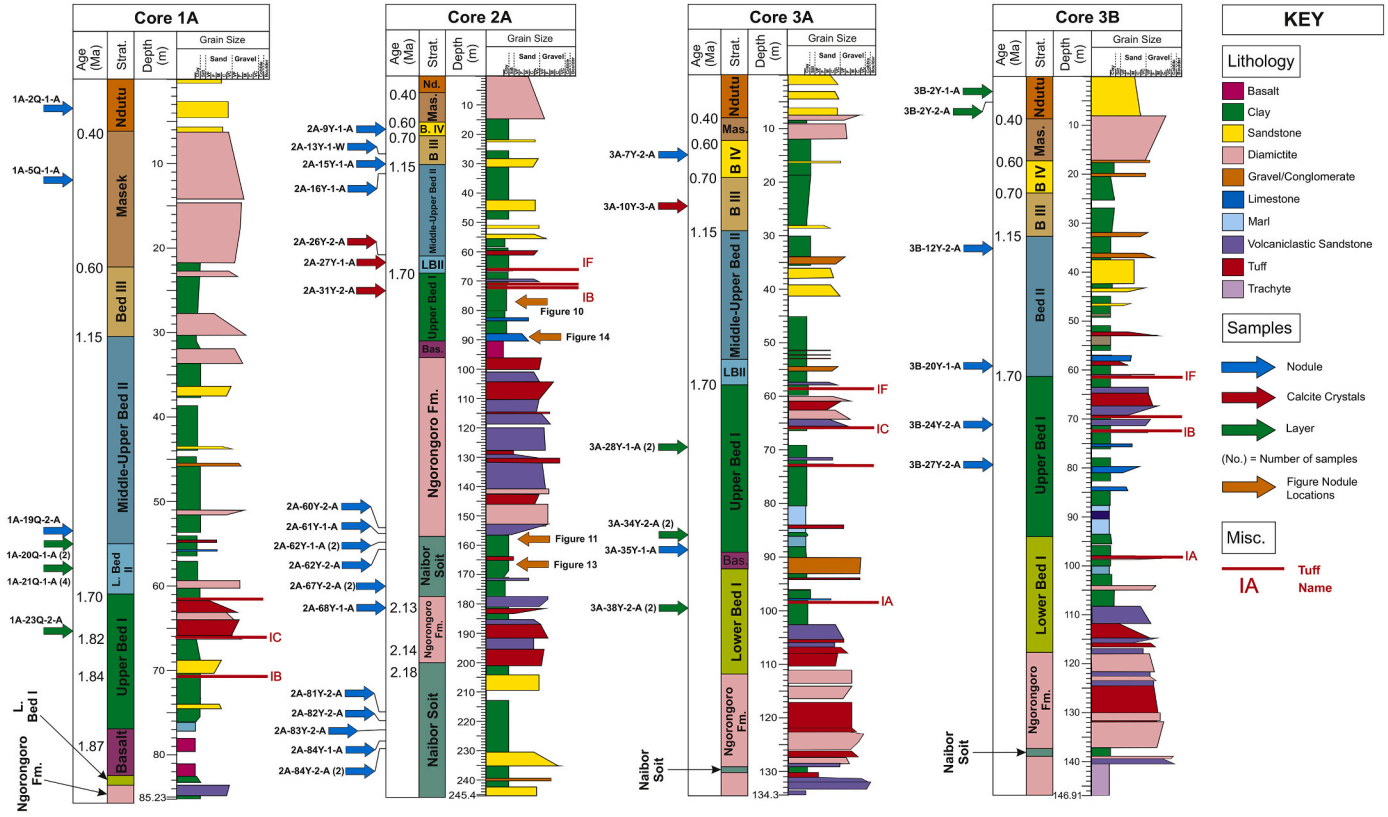

Fig. 7. Locations of nodular carbonate horizons, indicated by arrows, formed in vadose, groundwater interfacial or phreatic settings throughout cores 1A, 2A, 3A and 3B. Nodular carbonates occur in abundance throughout each core. Blue arrows indicate sample positions measured isotopically for Fig. 8. Orange arrows in Fig. 7 indicate positions of samples illustrated in other figures. (For interpretation of the references to colour in this figure legend, the reader is referred to the web version of this article.)

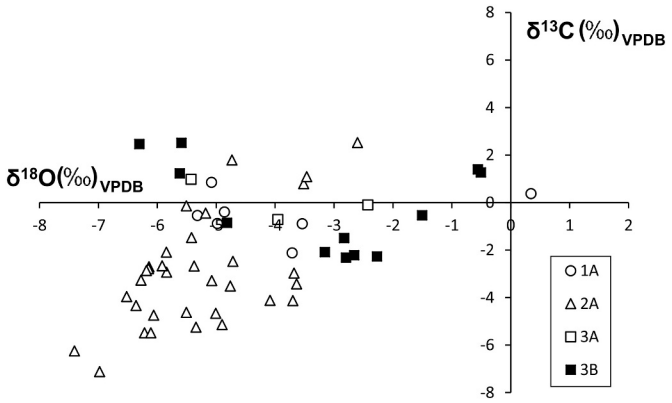

Fig. 8. Values of $\delta^{13}C$ plotted against $\delta^{18}O$ for Cores 1A, 2A and 3A, 3B from samples marked with blue and orange arrows in Fig. 7. Nodular isotope values show a co-variant trend also identified from lake-marginal areas by Cerling and Hay (1986), Sikes and Ashley (2007), Bennett et al. (2012) and Rushworth (2012), who interpreted them as of meteoric origin, forming predominantly in freshwater vadose and phreatic environments with evaporation and some mixing of saline-alkaline lake waters. (For interpretation of the references to colour in this figure legend, the reader is referred to the web version of this article.)

6. Interpretation

Conglomerates, sandstones and volcaniclastic sandstones represent fluvial and fluvio-deltaic sediments of sandy and gravelly braided streams (see detailed interpretations in Stanistreet et al., 2018b, 2018a, Stanistreet et al., 2020a, this volume). Claystones and sandy claystones represent settling of offshore and nearshore lake clays (Stanistreet et al., 2018a), with the sandy component due to contamination by wind-blown sand grains. Carbonate nodules formed as precipitated bodies within the claystone units. The micrite or dolmicrite carbonate layers associated with the lake clay facies represent hemipelagic to pelagic settings within the lake due to paucity of clay input. Such conditions were developed when lake flooding was maximal and clay sources were most remote from the depocentre. The tuffs were deposited variously from pyroclastic flows, ash surges, ash-falls (Stollhofen et al., 2008; Stollhofen and Stanistreet, 2012) and settling within the lake. Diamictities and sandy diamictites are mudflow deposits, generally lahars sourced from one of the nearby volcanic sources (Stanistreet et al., 2018a; de la Torre et al., 2018).

6.1. Primary depositional carbonate layers in Cores 1A, 2A, 3A

The dolmicrite to marl layer below Tuff IF (Figs. 3 and 4) records lake flooding (Stanistreet, 2012) prior to the hyperaridity recorded by Tuff IF (Stollhofen et al., 2008; Stanistreet et al., 2020b, this volume). The associated stevensitic claystone encountered between is of a type also recorded from FLK (= Frida Leakey Korongo) to HWK site outcrops (Fig. 1) by Hay and Kyser (2001) and Deocampo et al. (2017), and the precipitation of this neoformed clay would also have been promoted by the high-magnesium concentrations associated with the magnesium geochemical anomaly (Fig. 3, red double ended arrow) of Bed I, induced by terminal Ngorongoro basaltic volcanism (Stanistreet et al., 2020b this volume).

Bed I carbonate lithofacies layers tend to feather out and thin into clay facies towards the southeast (Fig. 3). At Borehole 1A only one carbonate layer is recorded, due to non-deposition, erosion or lapping of this facies onto the Bed I Basalt lava pile. As seen in the core (Fig. 5),

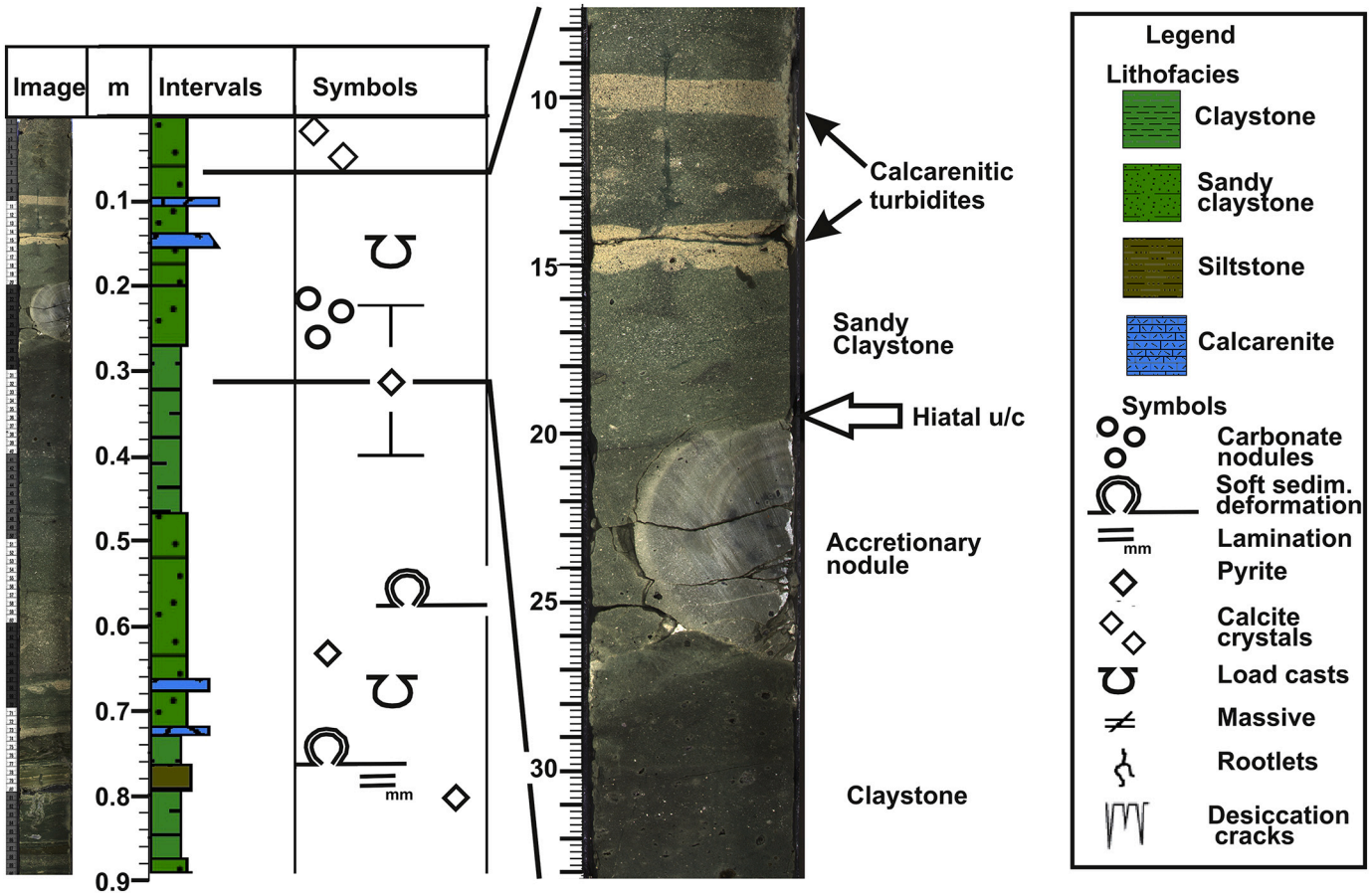

Fig. 9. Large (7.5 cm diameter) nodule from the middle of Upper Bed I in Borehole 2A (OGDP-OLD14-2A-33Y-1; see Figs. 2 and 7 for stratigraphic position). The nodule was precipitated in lake clays of the offshore lake after its withdrawal. Continued erosion then proceeded to erode clay down to and including the top of the nodule, prior to renewed lake flooding and deposition of nearshore sandy clays.

a typical carbonate layer has an eroded or incised top. Massive claystone grades upward through marl into the carbonate (in that case micritic limestone), representing deeper water palaeoenvironments. Immediately after the incised surface, subsequent surfaces are often erosional and might show desiccation cracking with some of them rooted. Pedogenic nodules can be present and frequently display layerwise concentrations. Although still lacustrine in nature, the palaeoenvironments are shallower and repeatedly subaerially exposed to allow desiccation, rooting, soil formation and meteoric water flushing. However, the sequence then grades upward once again into massive claystone facies, without such subaerial indicators, due to deepening conditions, and then might be followed by another carbonate layer which completes the deepening cycle (Figs. 4 and 5).

The rather special stromatolitic carbonate layer (Fig. 6) developed when the lake progressively transgressed onto the top basalt lava surface, under enhanced basin subsidence. The sedimentary sequence successively lapped onto the 5.7 m thick subaerial lava flow, a basalt unit which attained a maximum cumulative thickness of 21 m as multiple flows further to the east (Habermann et al., 2016). The lack of any pillow structures and hyaloclastites in both Olduvai outcrops and cores suggests that the lava flows were all subaerially emplaced in those areas and had cooled prior to lake transgression, so that there is no visible evidence of thermal lava/water interaction. It may have taken considerable time for the lake finally to transgress over the elevated lava surface, with the Ngorongoro sourced lavas having flowed across the already elevated Ngorongoro fan-delta surface. The onlapping sedimentary sequence is characterised by high organic carbon contents (> ~1% TOC) and abundant biomarkers derived from aquatic organisms (algae, cyanobacteria, sponges, macrophytes, etc.) (Colcord et al., 2018, 2019 this volume; Shilling et al., 2020, this volume). The stromatolitic lamination was generated by the accumulation of cyanobacterial mats displaying slightly domical structure. The bird's-eye structures (Fig. 6) indicate water-level variation and periodic drying of the cyanobacterial mat (Shinn, 1968), causing gas bubble development and its propagation between adjacent laminae. The stromatolitic layers just described represent a rare facies in the Olduvai Basin that relates directly to a shoreline, indicating that lake-level height usually varied continuously, and only rarely stabilised for any protracted time.

None of the Lower Bed I carbonates are present in Cores 1A and 2A, because a major (~75 kyr) disconformable hiatus developed between the Ngorongoro Formation and the Bed I Basalt (Fig. 3). To what extent erosion and/or onlap onto the topographic relief of the Ngorongoro Fan-delta played the major role in causing the hiatus is uncertain, but the topography of the fan surface certainly played a substantial part (Stanistreet et al., 2020a, this vol).

6.2. *Carbonates as shallow subsurface nodular precipitates in Cores 1A, 2A, 3A, 3B*

$\delta^{13}C$ and $\delta^{18}O$ isotope measurements (Fig. 8) from limestone nodules of the Palaeolake Olduvai depocentre (Fig. 1) display a range of values comparable to previous measurements from nodules of the lake marginal areas by Cerling and Hay (1986), Sikes and Ashley (2007), Bennett et al. (2012) and Rushworth (2012). But, it was initially surprising to find similar features associated with the deepest lake settings intersected by the boreholes. As was recognised in the previous studies, nodules displaying such isotopic signatures within lake marginal and distal fan sequences were formed in the near subsurface under the

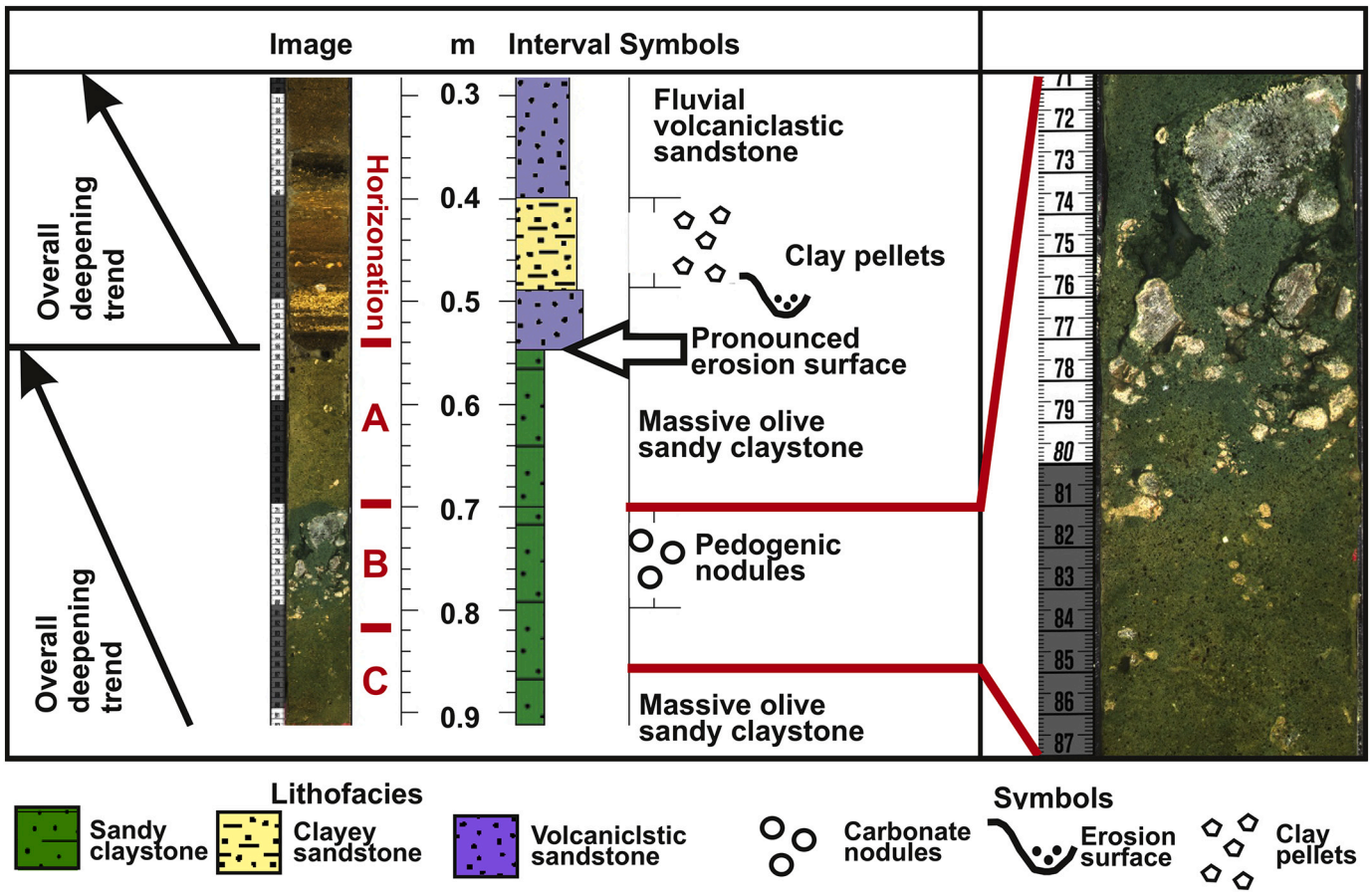

Fig. 10. Images of core and log with sedimentary descriptions, illustrating the location of a nodular profile in Core 2A-61Y-1 at 156.7 mbs near the top of the Naibor Soit Formation (see Figs. 2 and 7 for stratigraphic position). Red annotations A, B, C indicate soil horizonation, associated with the erosion/incision surface marking lake withdrawal. In this case the erosion surface was then covered by fluvial volcaniclastic sand. (For interpretation of the references to colour in this figure legend, the reader is referred to the web version of this article.)

influence of meteoric waters with relatively light $\delta^{18}O$ and $\delta^{13}C$ values. Contrastingly, outlier values which lie close to and either side of the zero value of $\delta^{18}O$ are isotopically enriched. These isotope values are representative of the mixing of meteoric waters (with relatively light $\delta^{18}O$ and $\delta^{13}C$ values) and lake waters from Palaeolake Olduvai (with comparatively heavy $\delta^{18}O$ and $\delta^{13}C$ values) during nodule growth, as previously recognised by Bennett et al. (2012). This signifies, however, that the lake-bed even in the deepest parts of the lake was occasionally exposed to the atmosphere, and that the lake dried out on at least 15 instances, recorded in Fig. 7.

Large calcitic accretionary nodules were studied by Bennett et al. (2012) and Rushworth (2012), and they reasoned that such nodules grew under phreatic conditions at tens of centimetres depth below the sediment surface. In the case of the nodule shown in Fig. 9 (2A-33Y-1), the overlying sequence then underwent erosion down to the depth of nodule formation, truncating the top of the nodule (labelled "hiatal u/c in Fig. 9). This shows that it formed soon after deposition of the host sediment. Subsequently, deposition of sandy claystone was punctuated by the emplacement of two calcarenitic turbidites.

Where multiple nodules grew to form a horizon (Fig. 10; core interval 2A-61Y-1) the calcite grains display a consistent extinction from their nucleus to their outermost rind when rotated in cross-polarised light, suggesting uniform palaeohydrological conditions throughout their growth. Nodules are characterised by fibrous, radial calcite grains enveloping pore space and sand grade grains of quartz (Fig. 11A and 11A1). Furthermore, the calcite grains co-occur with rinds of calcite cement that nucleate upon detrital quartz and feldspar grains. Quartz grains may be surrounded by several generations of calcite cements that are locally fed by calcite infilled cracks (Fig. 11B and 11B1). The nodular units show soil horizonation, with: a leached zone; zone of carbonate precipitation; and a zone of little enrichment. The olive sandy claystone, in which they developed, was deposited nearshore (Stanistreet, 2012; Stanistreet et al., 2018a). The lake then withdrew to induce development of a subaerial incision surface. Carbonate was precipitated below the exposed lake-bed and calcareous nodules formed at depths of tens of centimetres below that surface. In this case erosion did not proceed as deeply as the previously described nodular body, but instead the subaerial erosion surface was covered by fluvial sands associated with the progradation of the Ngorongoro Fan-delta (Stanistreet et al., 2020a, this volume). It should be noted that the pedogenic nodules act as visible markers for the overlying, but often less obvious erosional surface. When such a surface is more subtle, with perhaps claystone facies above and below the surface, horizons of carbonate precipitation can act as a witness to a cryptic hiatus within the sequence. Nodules of sample 2A-67Y-2 (59 cm to 73 cm), photomicrographs of which are shown in Fig. 11D and 11D1, are a case in point. They show vadose pedogenic alveolar textures, and yet the next obvious potentially hiatal surface is ~85 cm above, with intervening nodular horizons between. Thus, there is no obvious erosional or hiatal surface that relates to that specific horizon.

In the other horizon of nodules figured from core interval 2A-62Y-2 (Fig. 12), grains typically display grain-grain contacts without any apparent interstitial micrite matrix, instead they are bounded by significant pore space (Fig. 11C and 11C1), suggesting pedogenic formation above the groundwater table within the vadose zone. Such examples of the influence of vadose zone porewaters, and likely

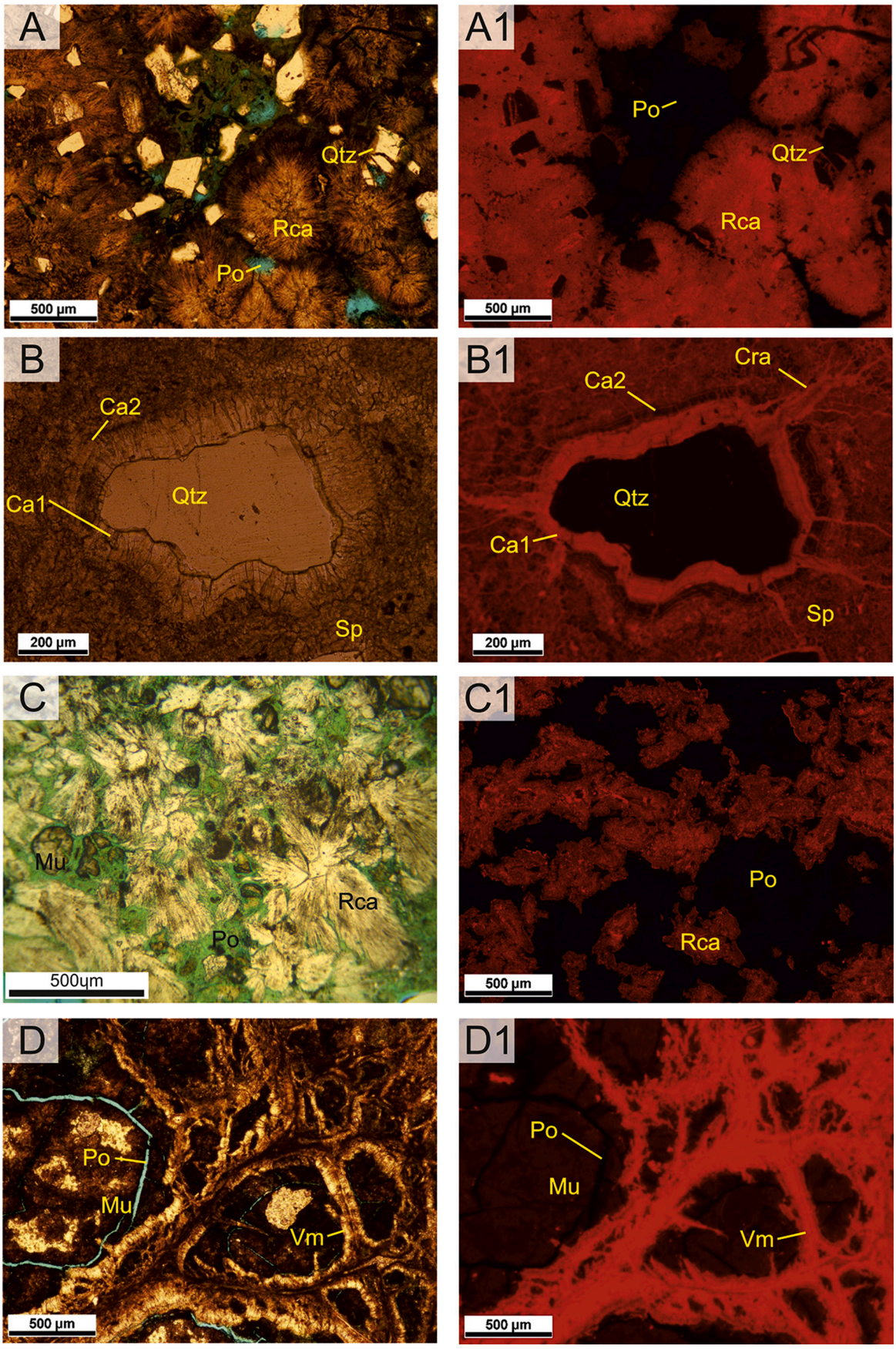

(caption on next page)

Fig. 11. (A) Optical and (A1) Cathodoluminescence photomicrographs of sample 2A-61Y-1 from Core 2A at 156.7 mbs, a nodule within the profile of Fig. 10, illustrating fibrous, radial calcite crystals filling pore space and enveloping sand grains of quartz, with calcite well distinguished from siliciclastic material under cathodoluminescence. (B) Optical and (B1) Cathodoluminescence images also from sample 2A-61Y-1 in Fig. 10 of a quartz grain surrounded by several generations of calcite cements that are locally fed by calcite-infilled cracks. Vadose nodule textures: (C) Optical and (C1) Cathodoluminescence photomicrographs from sample 2A-62Y-2 (Fig. 12) illustrating radial, fibrous calcite crystals, often with micrite envelopes, set within a matrix largely dominated by pore space and fine siliciclastic material. (D) and (D1): Optical and cathodoluminescene photomicrographs from sample 2A-67Y-2 (position indicated in Fig. 7) of strong alveolar textures, with calcite cements bounded by silts and clays. Qtz = Quartz, Po = Porosity, Rca = Radial/fibrous calcite precipitates, Sp = Sparite, Vm = Vadose micrite matrix, Mu = Various muds, Ca1 = Early stage calcite cement, Ca2 = Late stage calcite cement, Cra = Calcite infilled cracks.

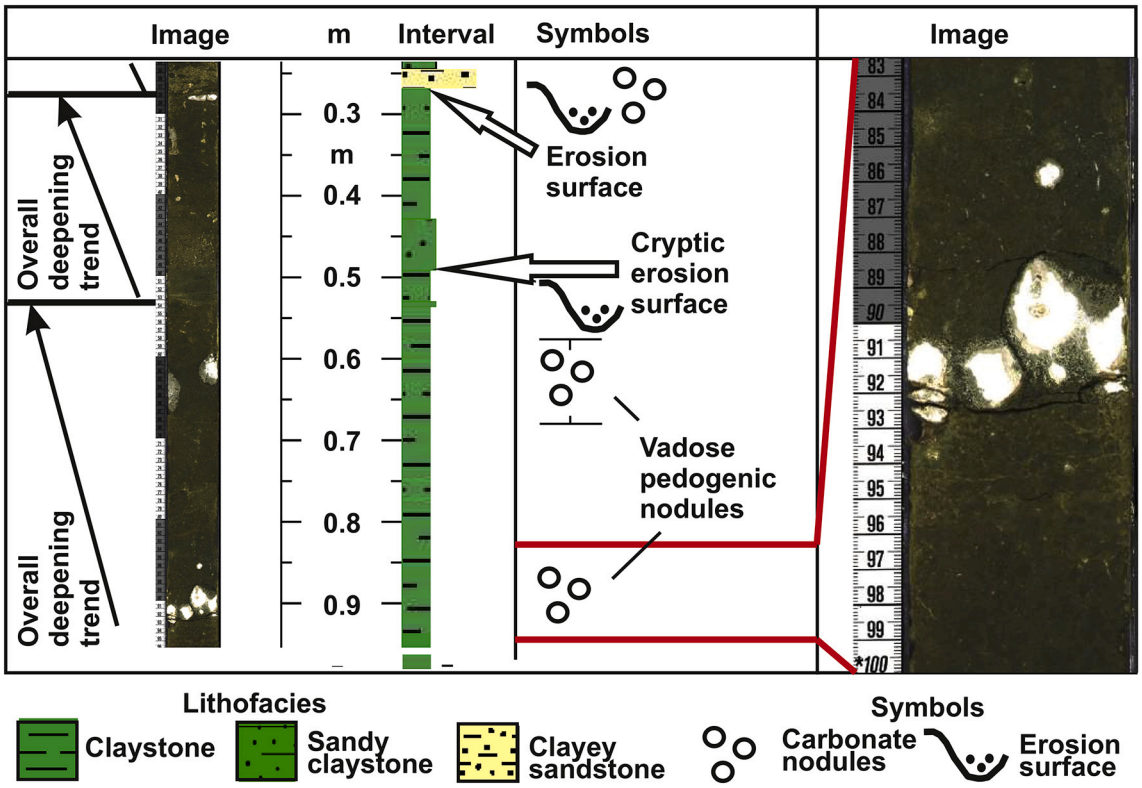

Fig. 12. Nodules from the Naibor Soit Formation of Core 2A, 161.2 mbs: Sample 2A-62Y-2 (88–93 cm; see Figs. 2 and 7 for stratigraphic position). Imaged core interval with sedimentary descriptions and graphic log showing the location of several small (< 3 cm) nodular carbonates, occurring in olive claystones and sandy claystones, and interpreted to have formed in a vadose setting based on petrological and petrographic characteristics.

associated pedogenesis (Ashley et al., 2014c), are further illustrated in Fig. 11D and 11D1. The latter is a spheroidal, medium sized (~5 cm diameter) carbonate nodule, occurring also in the Naibor Soit Formation, displaying strong evidence of vadose porewater interactions, pedogenesis, and serially repeated desiccation, including well-developed alveolar textures (Alonso-Zarza, 2003).

The specific enterolithic and chicken-wire nodular textures, illustrated from core intervals 2A-36Y-1 and 2 (Fig. 13), typically develop from sulphate evaporite precipitated in the shallow subsurface, usually comprising anhydrite or gypsum (Hussain and Warren, 1989). In the case here, the evaporite nodules were formed in lacustrine olive claystone within a depth range of 15 to 75 cm below the overlying hiatal erosion surface. Such structures are typically formed beneath marine or continental salt marsh settings. In support of this finding, McHenry et al. (2020b, this volume) detected rare gypsum in the core interval 2A-35Y-1 (48 cm–51 cm), immediately above those in Fig. 13. Sulphate pseudomorphs, in the form of calcite-replaced sulphate roses, have also been reported by Hay (1976), Bamford et al. (2008) and Bennett et al. (2012). In the case of the anhydritic forms figured here, the evaporites have been pseudomorphed subsequently by micritic calcite. During lake regression, the lake-bed emerged to form a salt marsh, to precipitate anhydrite/gypsum below the exposed surface. Micritic calcite subsequently replaced the evaporite under a meteoric rainwater regime and the erosional hiatal surface was preserved by the deposition of an overlying calcarenite layer and subsequent olive claystones and sandy claystones as the lake reflooded.

7. Discussion: Limestone and dolostone bodies as gauges of depth extremes in Palaeolake Olduvai

We contend that carbonate units and nodular horizons act as natural gauges of extremes of lake depth within the Olduvai Basin. As previously hypothesised (Stanistreet, 2012), primary carbonate layers are markers of lacustrine maximum flooding surfaces, in much the same way that limestones mark marine maximum flooding surfaces sequence stratigraphically in wholly marine shelf sequences (Van Wagoner et al., 1988). Nodular horizons on the other hand are markers of lake-bed emersion during extreme lake-level lowstands, when the lake was emptied and/or dried out. At such times rain fell onto the exposed lake-bed to form soil profiles or horizons in which nodules were precipitated within tens of centimetres below the surface, thus the resulting precipitates exhibit light isotopic values.

7.1. Lake level variation and resulting lacustrine stratigraphy

Layers of dolmicrite and micritic limestone are primary or dolomitised primary carbonate deposits during maximum flooding. At such times detrital clay sources were restricted most distant from the lake

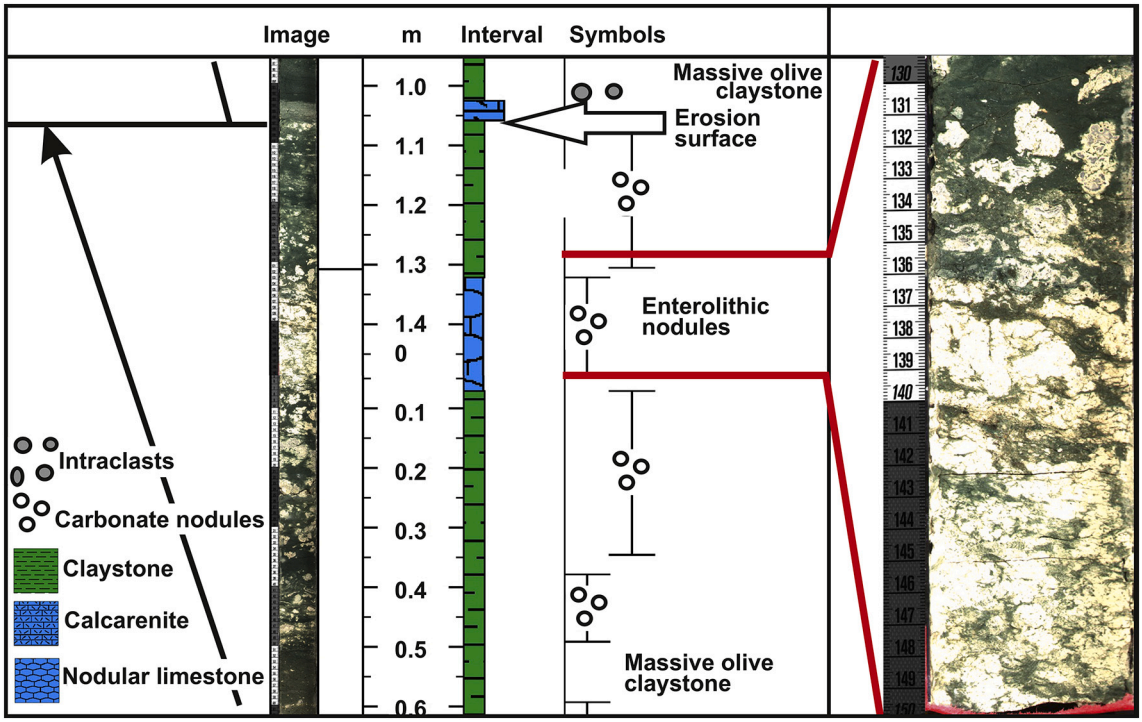

Fig. 13. Enterolithic to chickenwire textured calcite nodules intersected near the base of Upper Bed I in Borehole 2A (OGDP-OLD-2A-36Y-1 & 2; see Figs. 2 and 7 for stratigraphic position), here interpreted to have been subsequently pseudomorphed by micritic carbonate. (On the left hand scale 0.995 m to 1.400 m refers to measured positions in base of core interval OGDP-OLD-2A-36Y-1; 0 m to 0.602 m refers to measured positions in top of core interval OGDP-OLD-2A-36Y-2).

depocentre and the latter became starved of such clay input. This resulted in the onset of pelagic and hemipelagic settings in the deepest part of the lake, within which fine carbonate precipitates within the lake water column could accumulate with lesser or little detrital clay contamination to form micrite or marl layers.

An interpretation of how the primary carbonate facies encountered in Bed I developed is shown in Fig. 14. During a time of low lake-level (Fig. 14A), deepest Palaeolake Olduvai in the depocentre, bounded on the NW side by Fifth Fault, hosted mainly detrital facies. Detrital sediments entered from the south and east, spilling over the DK (= Douglas Korongo) Horst structural high (Fig. 1) to the point where sandy facies were deposited even within the depocentre. At such time, claystone and sandy claystone facies covered most of the depocentre and it was only adjacent to Fifth Fault that restricted pelagic settings existed and micritic carbonate sediments could accumulate. With a rise in lake-level (Fig. 14B, indicated by the blue arrows), associated with continuing subsidence along Fifth and other extensional faults (black half-arrow), the lake deepened and flooded over the lake marginal areas. Clay and sand source inputs were now more distant from the depocentre edge, and the pelagic setting expanded to include as much as half the depocentre area. Carbonate facies registered as far east as Borehole 3A, with the sequence accreting (red arrow) to fill the newly provided accommodation space. With a further rise of lake-level to maximum flooding (Fig. 14C), indicated by pairs of blue arrows, and continuing subsidence, lake waters flooded over the entire hinterland of the lake. Clay input sources were now most distant from the depocentre edge, and pelagic settings expanded over the depository, registering in the position of Borehole 2A and in the case of lowermost Upper Bed I, even as far southeast as Borehole 1A (see Fig. 3), when much of the depocentre must have been pelagic or hemipelagic. At such time of maximum flooding, micritic layers are even deposited in areas across Fifth Fault outside the depocentre, as recorded by Hay and Kyser (2001) at Loc. 80, Richard Hay Cliff, (Figs. 1 and 3) and visible in localities to the west.

The cycle just described succeeds a set of such cycles. Two previous cycles are shown in Fig. 14 indicating the pattern of facies repetition in the depocentre during Bed I. The main palaeoclimatic control on extremes of lake-level and cyclicity at that time was precessional variation in the monsoonal seasonality (Magill et al., 2013; Ashley et al., 2014b; Deocampo et al., 2017; Colcord et al., 2018, 2019; Stanistreet et al., 2020a, this vol), superposed upon lake-parasequential variations (Stanistreet, 2012; Colcord et al., 2018, 2019; Stanistreet et al., 2020b, this volume).

7.2. Carbonate layers, primary dolomites or dolomitised micrites?

Hay and Kyser (2001) studied dolomite layers from various depths in Bed I at Loc. 80, Richard Hay Cliff, and considered whether the layers were primary dolostones, or dolomitic neomorphic replacements of pre-existing micritic limestones. Much would depend upon the Mg^{2+}/Ca^{2+} ratio that could have been generated and maintained in the waters of Palaeolake Olduvai. The magnesium anomaly recognised by Stanistreet et al., 2020b, this volume), which promoted carbonate deposition, would have ensured that an overall high magnesium concentration developed in the lake, evident in the anomalously high magnesium content of the claystones and sandy claystones in that part of the sequence. This was related to a phase of basaltic magmatism that affected the basin, experienced as successive mafic tuffs, basaltic scoriaceous layers and a succession of complex basalt lava flows within the Bed I Basalt unit that would have provided high calcium (from plagioclase) as well as high magnesium concentrations. This was the basaltic culmination of the Ngorongoro bimodal volcanism (McHenry, 2012; Habermann et al., 2016). The anomalously high input of magnesium is also seen in the precipitation of “butter” claystones deposited within the lake (see Fig. 4), comprising largely stevensite, the magnesian endmember of the smectitic clay spectrum. Hay and Kyser (2001), Stollhofen et al. (2008), Stanistreet (2012) and Deocampo et al. (2017) suggest that such stevensite formed as a neomorphic precipitate in the saline-alkaline lake waters of Palaeolake Olduvai.

But, for primary dolmicrites or dolomitization of pre-existing

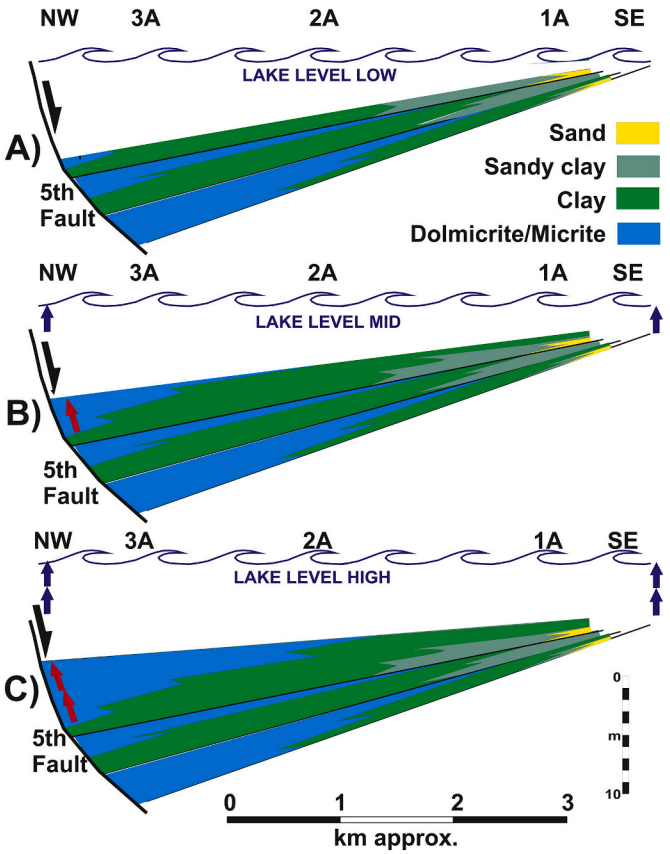

Fig. 14. Model scenarios of depositional changes with variations in lake depth, to explain the facies pattern changes and geometries exhibited in the lower half of Upper Bed I in Boreholes 1A, 2A and 3A (see Fig. 3). Carbonate layers develop in pelagic to hemipelagic settings adjacent to Fifth Fault in the deepest portion of the depocentre. Clay and some clastic input are from the toes of fan-deltas incident off the Ngorongoro Volcanic Highlands. Red arrows indicate incremental accretion of sediment associated with incremental deepening of the lake (shown by blue arrows), due to climatic changes in the presence of continued extensional subsidence. Half black arrows show polarity of downthrow on Fifth Fault (see Fig. 1). Indicative vertical scale only approximates amalgamated unit thickness and water depth. (For interpretation of the references to colour in this figure legend, the reader is referred to the web version of this article.)

calcitic micrites (Hay and Kyser, 2001; Rushworth, 2012) to proceed, the Mg^{2+}/Ca^{2+} ratio of the lake water would need to be raised (Folk and Land, 1975; Bathurst, 1976). For that to occur calcium would need to be fractionally removed from the input of weathering derived elements. The most likely sinks for calcium have been described in this paper. In the sebkha marine salt marshes of the Persian Gulf, anhydrite and gypsum are classic calcium sinks that locally elevate the Mg^{2+}/Ca^{2+} ratio in the porewaters (Bathurst, 1976). While there is plentiful evidence of sulphate precipitation in the basin (Hay, 1976) such as pseudomorphed gypsum roses (Bamford et al., 2008; Bennett et al., 2012), potential salt marsh precipitation of calcium sulphates (e.g., Fig. 13) was relatively rare and comprised low volumes within the basin as a whole. But, large volume sinks for calcium are the nodular horizons detailed in this paper. These are plentiful in the lake marginal areas and as shown here even developed within the lake depocentre. Thus, they may have played a major role in elevating the Mg^{2+}/Ca^{2+} ratio in the Olduvai basinal waters to promote dolomite as the predominant carbonate in the sequence, either primarily deposited or more likely through replacement. In this vein it is of interest to note that, from the Basalt to Tuff IB interval, McHenry et al. (2020b) record common and minor occurrences of aragonite in their XRD analyses of Core 2A and particularly Core 3A. Promotion of the precipitation of aragonite and inhibition of calcite is typical of waters comprising a high Mg^{2+}/Ca^{2+} ratio (e.g., Bathurst, 1976).

7.3. Limestone nodular horizons and hiatal/erosional surfaces when Palaeolake Olduvai dried out or emptied

The depocentre of Palaeolake Olduvai preserves many (> 15) horizons of carbonate nodules covering and even extending on the spectrum of nodule types recorded by Bennett et al. (2012) and Rushworth (2012). This large number was a surprise after it had been speculated that claystone and sandy claystone sequences would have been continuously deposited with few hiatuses. Nodules include micritic, fibrous, spherulitic, and sparry types, bearing features indicative of growth in vadose, groundwater interface, and phreatic settings. In some cases a distinct soil horizonation developed. Isotopic analysis of the nodules yielded a plot of $\delta^{13}C$ against $\delta^{18}O$ values that tallied with values previously measured in the lake marginal and fan toe palaeoenvironments of the Olmoti Fan system (Cerling and Hay, 1986; Sikes and Ashley, 2007; Bennett et al., 2012; Rushworth, 2012), interpreted to indicate their formation under meteoric freshwater conditions, with some mixing of isotopically heavier saline-alkaline lake waters.

In most cases nodular layers relate to overlying erosional incision or hiatal surfaces, of which the latter might be subtly developed where clay facies are deposited after hiatus on top of similar underlying clay facies. In many cases (e.g. Fig. 10; 2A-61Y-1: 54.5 cm) the erosion surface is more obviously preserved. Nodular horizons are contained within individual lake-parasequences, which have a recurrence interval of 4 kyr-6 kyr average (Stanistreet, 2012; Bennett et al., 2012; Stanistreet et al., 2018b; de la Torre et al., 2018), providing an indication of the maximum time available for nodular horizon development. This would be on the order of a few millennia, taking into account the time required for the sedimentation of the 50 cm to 150 cm thick parasequential unit, itself (Stanistreet, 2012; Bennett et al., 2012), in the first place. More pronounced incision surfaces in Bed I mark more extended hiatal gaps in a spectrum up to tens of thousands of years. For example, the incision surface that excludes Lower Bed I from Cores 1A and 2A (Fig. 3) extends for ~ 75 kyr (Stanistreet et al., 2020b, this volume) and the Crocodile Valley Incision Surface also shown in Fig. 3 within Lower Bed II extends for > 8 parasequences (Stanistreet, 2012), or a time span of ~40 kyr. Such pronounced lake-level falls, causing major incision, could be accommodated within the closed Olduvai Basin, but if enhanced erosion surfaces are encountered in the depocentre, there is a possibility that at such times regional drainages were connecting the Olduvai depository to neighbouring drainages due to tectonic activity. In that case the most likely connection would have been through to the adjacent Lake Natron Basin (Hay, 1976).

Nodular horizons in the depocentre area of Palaeolake Olduvai (Fig. 1) mark periods of extreme lake-level fall, when the exposed lakebed could experience and receive rainfall even within its formerly deepest parts. Calcareous material was leached and precipitated at depths of tens of centimetres below the surface to form weak or more mature soil horizons in vadose settings, or more regular accretionary spheroidal nodules in more waterlogged areas at the groundwater interface or in phreatic settings. In one case (Fig. 13) salt marshes developed on the emersed lake-bed, to precipitate Ca-sulphates below surface, in the form of enterolithic nodular bodies that were subsequently pseudomorphed by micritic calcite.

8. Conclusions

Carbonate facies intersected in boreholes drilled into the Palaeolake Olduvai depocentre are of three main types: (1) Dolmicrites, micrites and marls representing primary depositional layers, (2) nodular to amalgamated nodular limestones precipitated shallowly below the

sedimentary surface in vadose pedogenic, groundwater interface, or phreatic groundwater settings; and (3) thin calcarenite layers often normally graded with underlying erosion. The layers (1) mark periods of maximum flooding when the lake expanded across its hinterland and over fan-delta surfaces incident from the Ngorongoro Volcanic Highlands. The carbonate units were deposited in pelagic or hemipelagic settings due to their distal position from those detrital sediment sources. By contrast, the nodular bodies (2) show meteoric (rainfall) isotope values, indicating times when the lake emptied and/or dried out, when carbonates were precipitated under the influence of rainfall beneath the abandoned lake surface, now marked as a hiatus or hiatal disconformity that can usually be identified. The calcarenites (3) represent deposits of low density turbidity currents, but this facies might also develop as erosional crystal lag deposits.

The fine carbonate layers form at the top of lake-parasequence cycles prior to lake withdrawal. This was followed by shallowing, under which conditions, an erosion surface formed prior to the deposition of the next cycle. Clusters of such carbonate layers mark times when the overall lake level was relatively high, marking precessional wet phases. These Palaeolake Olduvai carbonate layers formed only during a time period when there was a magnesium anomaly developed in lake claystone, sandy claystone and butter (stevensitic high-Mg) claystone facies. During that period basaltic magmatism dominated the basin and mafic tuffs and basalts were erupted and extruded to provide magnesium and calcium in abundance. The predominance of dolomite, either primary, or a product of dolomitization, would indicate that high Mg^{2+}/Ca^{2+} ratios prevailed. Calcium was most likely partitioned into calcic evaporites such as anhydrite or gypsum, and also into palaeosol profiles and nodular horizons.

There are a large number of hiatal surfaces marked by nodules and nodular pedogenic profiles throughout the lacustrine portions of the Olduvai Beds and these mark discontinuities in the otherwise mostly fine-grained facies sequences. A minimum of 15 surfaces are counted, signifying when rainfall directly affected the abandoned lake-bed in its depocentre. Single nodular horizons within a lake-parasequence mark hiatuses lasting a few millennia, while some better developed nodular profiles would require several to many thousands of years to form. The latter often sit beneath obvious incisional disconformities, some covered by fluvial sediments, that would also point to a longer period of lake abandonment at that locale in that instance. Such hiatuses need be taken into account in the construction of age-depth models, subsidence curves, and calculation of sedimentation rates. In the OGCP boreholes this is particularly the case, where the shorter hiatuses just discussed are joined by major hiatal disconformities extending to ~ 40 kyr (Crocodile Valley Incision Surface in Core 1A) and 75 kyr (incision surface below the Bed I Basalt in Cores 1A and 2A).

Declaration of Competing Interest

Please check the following as appropriate:

- o All authors have participated in (a) conception and design, or analysis and interpretation of the data; (b) drafting the article or revising it critically for important intellectual content; and (c) approval of the final version.
- o This manuscript has not been submitted to, nor is under review at, another journal or other publishing venue.
- o The authors have no affiliation with any organization with a direct or indirect financial interest in the subject matter discussed in the manuscript

Acknowledgements

We are most grateful to Jim Marshall for his guidance and inspiration during the development of this project. Sincere thanks are due to Steve Crowley, University of Liverpool Stable Isotope Laboratory, for his assistance with the preparation and analysis of carbonates studied in this paper. We are grateful to the Tanzanian institutions that permitted and co-operated with OGCP's research, including the Tanzanian Commission for Science and Technology (COSTECH), the Tanzanian Department of Antiquities and Ngorongoro Conservation Area Authority (NCAA). The Stone Age Institute funded the Olduvai Gorge Coring Project (OGCP), with support from the Kamen Foundation, the Gordon and Ann Getty Foundation, the John Templeton Foundation, the Fred Maytag Foundation, and Kay and Frank Woods. Project funding came from the National Science Foundation (BCS grant #1623884 to Njau and McHenry) and the Stone Age Institute. We are grateful for additional funding from Indiana University, Bloomington (JKN), the Stone Age Institute (JKN and IGS), the Palaeontological Scientific Trust (PAST) (JKN, IGS and HS). Anders Noren, Kristina Brady, Brian Grivna, and staff of the University of Minnesota LacCore facility were willing and essential participants in supervising the logging and sampling of the core. We are very grateful for important discussions with many members of the OGCP team, including Lindsay McHenry and Al Deino. The text was improved immensely by the diligent overviews of four anonymous referees and editors Thomas Algeo and Lindsay McHenry.

Appendix A. Supplementary data

Supplementary data to this article can be found online at https://doi.org/10.1016/j.palaeo.2020.110032.

References

Alonso-Zarza, A., 2003. Palaeoenvironmental significance of palustrine carbonates and calcretes in the geological record. Earth Sci. Rev. 60, 261–298.

Ashley, G.M., Emily, J., Beverly, E.J., Sikes, N.E., Driese, S.G., 2014a. Paleosol diversity in the Olduvai Basin, Tanzania: Effects of geomorphology, parent material, depositional environment, and groundwater on soil development. Quat. Int. 322-323, 66–77.

Ashley, G.M., De Wet, C.B., Dominguez-Rodrigo, M., Karis, A.M., O'Reilly, T.M., Baluyot, R., 2014b. Freshwater limestone in an arid basin: a goldilocks effect. J. Sediment. Res. 84, 988–1004.

Ashley, G., Beverly, E., Sikes, N., Driese, S., 2014c. Paleosol diversity in the Olduvai Basin, Tanzania: Effects of geomorphology, parent material, depositional environment, and groundwater on soil development. Quat. Int. 322-323, 66–77.

Bamford, M.K., Stanistreet, I.G., Stollhofen, H., Albert, R.M., 2008. Late Pliocene grassland from Olduvai Gorge, Tanzania. Palaeogeogr. Palaeoclimatol. Palaeoecol. 257, 280–293.

Bathurst, R.G.C., 1976. Carbonate sediments and their diagenesis. In: Developments in Sedimentology 12. Science, Elsevier (657pp).

Bennett, C.E., Marshall, J.D., Stanistreet, I.G., 2012. Carbonate horizons, paleosols, and lake flooding cycles: Beds I and II of Olduvai Gorge, Tanzania. J. Hum. Evol. 63, 328–341.

Blumenschine, R.J., Masao, F.T., Stollhofen, H., Stanistreet, I.G., Bamford, M.K., Albert, R.M., Njau, J.K., Prassack, K.A., 2012b. Landscape distribution of Oldowan stone artifact assemblages across the fault compartments of the eastern Olduvai Lake Basin during early lowermost Bed II times. In: Blumenschine, R.J., Masao, F.T., Stanistreet, I.G., Swisher, C.C. (Eds.), Five Decades after *Zinjanthropus* and *Homo habilis*: Landscape Paleoanthropology of Plio-Pleistocene Olduvai Gorge, Tanzania. J. Hum. Evol, vol. 63. pp. 384–394.

Blumenschine, R.J., Stanistreet, I.G., Njau, J.K., Bamford, M.K., Masao, F.T., Albert, R.M., Stollhofen, H., Andrews, P., Prassack, K.A., McHenry, L.J., Fernandez-Jalvo, Y., Camilli, E.L., Ebert, J.I., 2012a. Environments and activity traces of hominins across the FLK Peninsula during Zinjanthropus times (1.84 Ma), Olduvai Gorge, Tanzania. In: Blumenschine, R.J., Masao, F.T., Stanistreet, I.G., Swisher, C.C. (Eds.), Five Decades after *Zinjanthropus* and *Homo habilis*: Landscape Paleoanthropology of Plio-Pleistocene Olduvai Gorge, Tanzania. J. Hum. Evol, vol. 63. pp. 364–383.

Cerling, T.E., Hay, R.L., 1986. An isotopic study of paleosol carbonates from Olduvai Gorge. Quat. Res. 25, 63–78.

Cohen, A.S., Stone, J., Beuning, K., Park, L., Reinthal, P., Dettman, D., Scholz, C.A., Johnson, T., King, J.W., Talbot, M., Brown, E., Ivory, S., 2007. Ecological Consequences of early late-pleistocene megadroughts in Tropical Africa. Proc. Natl. Acad. Sci. 104, 16422–16427.

Colcord, D.E., Shilling, A.M., Sauer, P.E., Freeman, K.H., Njau, J.K., Stanistreet, I.G., Stollhofen, H., Schick, K.D., Toth, N., Brassell, S.C., 2018. Sub-Milankovitch paleoclimatic and paleoenvironmental variability in East Africa recorded by Pleistocene lacustrine sediments from Olduvai Gorge, Tanzania. Palaeogeogr. Palaeoclimatol. Palaeoecol. 495, 284–291. https://doi.org/10.1016/j.palaeo.2018.01.023.

Colcord, D.E., Shilling, A.M., Freeman, K.H., Njau, J.K., Stanistreet, I.G., Stollhofen, H., Schick, K.D., Toth, N., Brassell, S.C., 2019. This volume. Aquatic biomarkers records

of Pleistocene environmental changes at Paleolake Olduvai, Tanzania. Palaeogeogr. Palaeoclimatol. Palaeoecol. https://doi.org/10.1016/j.palaeo.2018.01.023.
de la Torre, I., Albert, R.M., Macphail, R., McHenry, L.J., Pante, M.C., Rodríguez-Cintas, A., Stanistreet, I.G., Stollhofen, H., 2018. The contexts and early Acheulean archaeology of the EF-HR palaeo-landscape (Olduvai Gorge, Tanzania). J. Hum. Evol. 120, 274–297.
Deino, A.L., 2012. $^{40}Ar/^{39}Ar$ dating of Bed I, Olduvai Gorge, Tanzania, and the chronology of early Pleistocene climate change. In: Blumenschine, R.J., Masao, F.T., Stanistreet, I.G., Swisher, C.C. (Eds.), Five Decades after *Zinjanthropus* and *Homo habilis*: Landscape Paleoanthropology of Plio-Pleistocene Olduvai Gorge, Tanzania. J. Hum. Evol, vol. 63. pp. 252–273.
Deino, A.L., King, J., McHenry, L.J., Stanistreet, I.G., Stollhofen, H., Toth, N., Schick, K., Njau, J.K., 2020. Chronostratigraphy and Age Modeling of Quaternary Drill Cores from the Olduvai Basin, Tanzania (Olduvai Gorge Coring Project). Palaeogeogr. Palaeoclimatol. Palaeoecol In review (this volume).
Deocampo, D.M., Berry, P.A., Beverly, E.J., Ashley, G.M., Jarrett, R.E., 2017. Whole-rock geochemistry tracks precessional control of Pleistocene lake salinity at Olduvai Gorge, Tanzania: a record of authigenic clays. Geology. https://doi.org/10.1130/G38950.1. G38950–1.
Folk, R.L., Land, L.S., 1975. Mg/Ca Ratio and Salinity: two Controls over Crystallization of Dolomite. Am. Assoc. Pet. Geol. Bull. 59, 60–68.
Habermann, J.M., McHenry, L.J., Stollhofen, H., Tolosana-Delgado, R., Stanistreet, I.G., Deino, A.L., 2016. Discrimination, correlation, and provenance of Bed I tephrostratigraphic markers, Olduvai Gorge, Tanzania, based on multivariate analyses of phenocryst compositions. Sediment. Geol. 339, 115–133.
Hay, R.L., 1976. Geology of the Olduvai Gorge. California Press, Berkeley, California (203pp).
Hay, R.L., Kyser, T.K., 2001. Chemical sedimentology and paleoenvironmental history of Lake Olduvai, a Pliocene lake in northern Tanzania. Geol. Soc. Am. 113, 1505–1521.
Hussain, M., Warren, J.K., 1989. Nodular and enterolithic gypsum: the "sabkha-tization" of Salt Flat playa, west Texas. Sediment. Geol. 64, 13–24.
Leakey, M.D., 1971. Olduvai Gorge 3: Excavations in Beds I and II 1960–1963. Cambridge University Press, Cambridge (306 pp).
Leakey, M.D., Roe, D.A., 1994. Olduvai Gorge 5: Excavations in Beds III, IV and the Masek Beds, 1968-1971. Cambridge University Press, Cambridge.
Liutkus, C.M., Ashley, G.M., Sikes, N.E., Wright, J.D., 2005. Paleoenvironmental interpretation of lake-margin deposits using $\delta^{13}C$ and $\delta^{18}O$ results from early Pleistocene carbonate rhizocretions, Olduvai Gorge, Tanzania. Geology 33, 377–380.
Lu, K., Hanafy, S., Stanistreet, I.G., Njau, J., Schick, K., Toth, N., Stollhofen, H., Schuster, G., 2019. Seismic imaging of the Olduvai Basin. Palaeogeogr. Palaeoclimatol. Palaeoecol. https://doi.org/10.1016/j.palaeo.2019.109246. this volume.
Magill, C.R., Ashley, G.M., Freeman, K.H., 2013. Ecosystem variability and early human habitats in eastern Africa. Proc. Natl. Acad. Sci. 110, 1167–1174.
Maslin, M.A., Brierley, C.M., Milner, A.M., Shultz, S., Trauth, M.H., Wilson, K.E., 2014. East African climate pulses and early human evolution, commissioned review paper. Quat. Sci. Rev. 101, 1–17.
McHenry, L.J., 2012. A revised stratigraphic framework for Olduvai Gorge Bed I based on tuff geochemistry. In: Blumenschine, R.J., Masao, F.T., Stanistreet, I.G., Swisher, C.C. (Eds.), Five Decades after Zinjanthropus and Homo Habilis: Landscape Paleoanthropology of Plio-Pleistocene Olduvai Gorge, Tanzania. J. Hum. Evol. vol, vol. 63. pp. 284–299.
McHenry, L.J., Stanistreet, I.G., Stollhofen, H., Njau, J., Toth, N., Schick, K., 2020a. Tuff fingerprinting and correlations between OGCP cores and outcrops for Pre-Bed I and Bed I/II at Olduvai Gorge, Tanzania. Palaeogeogr. Palaeoclimatol. Palaeoecol. https://doi.org/10.1016/j.palaeo.2020.109630. This volume.
McHenry, L., Kodikara, G., Stanistreet, I.G., Stollhofen, H., Njau, J., Toth, N., Schick, K., 2020b. Lake conditions and detrital sources of Paleolake Olduvai, Tanzania, reconstructed using X-Ray Diffraction analysis of cores. Palaeogeogr. Palaeoclimatol. Palaeoecol. https://doi.org/10.1016/j.palaeo.2020.109855. This volume.
Mollel, G.F., Swisher III, C.C., 2012. The Ngorongoro Volcanic Highland and its relationships to volcanic deposits at Olduvai Gorge and East African Rift volcanism. J. Hum. Evol. 63, 274–283.
Rushworth, E., 2012. Carbonates from Olduvai Gorge, Tanzania: Palaeohydrology and Geochronology. Doctoral thesis. University of Liverpool.
Scholz, C.A., Johnson, T.C., Cohen, A.S., King, J.W., Peck, J.A., Overpeck, J.T., Talbot, M.R., Brown, E.T., Kalindekafe, L., Amoako, P.Y.O., Lyons, R.P., Shanahan, T.M., Castaneda, I.S., Heil, C.W., Forman, S.L., McHargue, L.R., Beuning, K.R., Gomez, J., Pierson, J., 2007. East African megadroughts between 135-75 kyr ago and bearing on early-modern human origins. Proc. Natl. Acad. Sci. 104, 16416–16421.
Shilling, A.M., Colcord, D.E., Karty, J., Hansen, A., Freeman, K.H., Njau, J.K., Stanistreet, I.G., Stollhofen, H., Schick, K., Toth, N., Brassell, S.C., 2020. Biogeochemical evidence from OGCP Core 2A for environmental and climatic changes in the Olduvai Basin preceding deposition of Tuff IB. Palaeogeog., Palaeoclimat., Palaeoecol., this volume.
Shinn, E.A., 1968. Practical significance of birdseye structures in carbonate rocks. J. Sediment. Petrol. 38, 215–223.
Sikes, N.E., Ashley, G.M., 2007. Stable isotopes of pedogenic carbonates as indicators of paleoecology in the Plio-Pleistocene (Upper Bed I), western margin of the Olduvai basin, Tanzania. J. Hum. Evol. 53, 574–594.
Stanistreet, I.G., 2012. Fine resolution of early hominin time, Beds I and II, Olduvai Gorge, Tanzania. In: Blumenschine, R.J., Masao, F.T., Stanistreet, I.G., Swisher, C.C. (Eds.), Five Decades after *Zinjanthropus* and *Homo habilis*: Landscape Paleoanthropology of Plio-Pleistocene Olduvai Gorge, Tanzania. J. Hum. Evol, vol. 63. pp. 300–308.
Stanistreet, I.G., McHenry, L.J., Stollhofen, H., De La Torre, I., 2018b. Bed II Sequence stratigraphic context of EF-HR and HWK EE archaeological sites, and the Oldowan/Acheulean succession at Olduvai Gorge, Tanzania. J. Hum. Evol. 120, 19–31.
Stanistreet, I.G., Stollhofen, H., Deino, A., McHenry, L., Toth, N., Schick, K., Njau, J., 2020a. This volume. New Olduvai Basin stratigraphy and stratigraphic concepts revealed by OGCP cores into the Palaeolake Olduvai depocentre, Tanzania. Palaeogeogr. Palaeoclimatol. Palaeoecol. https://doi.org/10.1016/j.palaeo.2020.109751.
Stanistreet, I.G., Boyle, J.F., Stollhofen, H., Deocampo, D., Deino, A., McHenry, L., Toth, N., Schick, K., Njau, J., 2020b. Palaeosalinity and palaeoclimatic geochemical (elements Ti, Mg, Al) proxies vary with Milankovitch cyclicity, Beds I and II in OGCP cores, Palaeolake Olduvai, Tanzania. Palaeogeogr. Palaeoclimatol. Palaeoecol. https://doi.org/10.1016/j.palaeo.2020.109656. this volume.
Stanistreet, I.G., Stollhofen, H., Njau, J.K., Farrugia, P., Pante, M.C., Masao, F.T., Albert, R.M., Bamford, M.K., 2018a. Lahar inundated, modified and preserved 1.88 Ma early hominin (OH24 and OH56) Olduvai DK site. J. Hum. Evol. 116, 27–42.
Stollhofen, H., Stanistreet, I.G., 2012. Plio-Pleistocene syn-sedimentary fault compartments underpin lake margin paleoenvironmental mosaic, Olduvai Gorge, Tanzania. In: Blumenschine, R.J., Masao, F.T., Stanistreet, I.G., Swisher, C.C. (Eds.), Five Decades after Zinjanthropus and Homo Habilis: Landscape Paleoanthropology of Plio-Pleistocene Olduvai Gorge, Tanzania. J. Hum. Evol. vol, vol. 63. pp. 309–327.
Stollhofen, H., Stanistreet, I.G., McHenry, L.J., Mollel, G.F., Blumenschine, R.J., Masao, F.T., 2008. Fingerprinting facies of the Tuff IF marker, with implications for early hominin palaeoecology, Olduvai Gorge, Tanzania. Palaeogeogr. Palaeoclimatol. Palaeoecol. 259, 382–409.
Trauth, M.H., 2014. A new probabilitistic technique to determine the best age model for complex stratigraphic sequences. Quat. Geochronol. 22, 65–71.
Trauth, M.H., Bergner, A.G.N., Foerster, V., Junginger, A., Maslin, M.A., Schaebitz, F. Trauth, et al., 2015. Episodes of environmental stability versus instability in late Cenozoic lake records of Eastern Africa. J. Hum. Evol. 87, 21–31.
Van Wagoner, J.C., Posamentier, H.W., Mitchum Jr., R.M., Vail, P.R., Sarg, J.F., Loutit, T.S., Hardenbol, J., 1988. An overview of the fundamentals of sequence stratigraphy and key definitions. In: Wilgus, C.K., Hastings, B.S., Kendall, C.G.St.C., Posamentier, H.W., Ross, C.A., Van Wagoner, J.C. (Eds.), Sea Level Changes - an Integrated Approach. SEPM Special Publication, vol. 42. pp. 39–45.